

NASA Technical Paper 1649

Navigation, Guidance, and Control for Helicopter Automatic Landings

James R. Kelly and Frank R. Niessen

MAY 1980





NASA Technical Paper 1649

Navigation, Guidance, and Control for Helicopter Automatic Landings

James R. Kelly and Frank R. Niessen
Langley Research Center
Hampton, Virginia



National Aeronautics
and Space Administration

**Scientific and Technical
Information Office**

1980

SUMMARY

One of the major goals of NASA Langley Research Center's VTOL Approach and Landing Technology (VALT) Program was to develop the capability for performing decelerating approaches and landings under instrument meteorological conditions. In pursuing this goal, it was necessary to develop a navigation, guidance, and control concept for helicopter automatic approach and landings. Flight tests of the basic concept were initiated in 1969 with a CH-46C variable-stability helicopter. The first fully automatic approach and landings were accomplished in February 1972. In 1977, the CH-46C was replaced by a CH-47B variable-stability helicopter equipped with a general-purpose digital flight computer which was used to implement the advanced automatic approach and landing concept described in this report.

The primary focus of this report is on the navigation, guidance, and control algorithms employed in the automatic landing concept. Certain aspects of the digital implementation will be discussed, including critical sensor compensation requirements. Data will be shown to illustrate system performance during fully automatic approach and landings in a variety of wind conditions.

INTRODUCTION

One of the major goals of NASA Langley Research Center's VTOL Approach and Landing Technology (VALT) Program was to develop the capability for performing decelerating approaches and landings under instrument meteorological conditions (IMC). In pursuing this goal, it was necessary to develop a navigation, guidance, and control concept for helicopter automatic approach and landings. Flight tests of the basic concept were initiated in 1969 with a CH-46C variable-stability helicopter. The results of this investigation, which involved pilot-controlled approaches using a 3-cue flight director, were reported in reference 1. The first fully automatic approach and landings were accomplished 3 yr later, in February 1972, with a refined version of the concept as described in reference 2.

During all of the decelerating approach and landing studies conducted with the CH-46C helicopter, the navigation and guidance laws were implemented using general-purpose, onboard, analog computers. Operationally oriented features such as airspeed-to-groundspped transition logic were not incorporated due to limited onboard computing capacity.

In 1977, the CH-46C was replaced by the CH-47B variable-stability helicopter described in reference 3. The CH-47B research system included a general-purpose digital flight computer which was used, in part, to implement the navigation, guidance, and control laws for the automatic approach and landing concept. In converting the implementation from analog to digital, many refinements and operational features were incorporated. These features were

subsequently evaluated and refined and resulted in the navigation, guidance, and control concept reported herein.

The primary focus of this report is on the navigation, guidance, and control algorithms employed in the automatic landing concept. Certain aspects of the digital implementation will be discussed, including critical sensor compensation requirements. Data will be shown to illustrate system performance during fully automatic approach and landings in a variety of wind conditions.

SYMBOLS AND ABBREVIATIONS

Values are given in both SI and U.S. Customary Units. The measurements and calculations were made in U.S. Customary Units.

A	area under curve of acceleration plotted as function of range, m^2/sec^2 (ft^2/sec^2)
a_x, a_y, a_z	body-mounted accelerometer outputs, m/sec^2 (ft/sec^2)
a_z'	intermediate term in the transformation equations, m/sec^2 (ft/sec^2)
CDU	control display unit
DIU	digital interface unit
ECS	electronic control system
E_i	input signal to limiter
E_o	output signal from limiter
GSE	groundspeed error
g	gravity constant, $9.8 \text{ m}/\text{sec}^2$ ($32.2 \text{ ft}/\text{sec}^2$)
H	altitude, m (ft)
IMC	instrument meteorological conditions
I/O	input/output
K_1, K_2, \dots, K_{22}	system gains
L	limit value
LTS	laser tracking system
m	mass, kg (slugs)
s	Laplacian operator

T	sample period, sec
TDS	transponder data system
TIU	TDS interface unit
V	airspeed, m/sec (ft/sec)
V_h	component of airspeed in horizontal plane, m/sec (ft/sec)
V_{GS}	groundspeed, m/sec (ft/sec)
$\frac{Y_v}{m}$	aircraft side drag term, 1/sec
$\dot{x}_h, \dot{y}_h, \dot{z}_h$	aircraft velocity in local level coordinate frame, m/sec (ft/sec)
X, Y, Z	aircraft displacement in runway reference coordinate frame (see fig. 3), m (ft)
$\hat{x}_d, \hat{y}_d, \hat{z}_d$	dead-reckoning position estimates in runway reference coordinate frame, m (ft)
\hat{x}_w, \hat{y}_w	components of estimated wind in runway reference coordinate frame, m/sec (ft/sec)
y_v	side force proportional to side-force velocity, N/m/sec (lb/ft/sec)
β	sideslip angle, rad
Γ	ground track angle, rad
ζ	damping ratio
θ	pitch attitude, positive nose upward, deg
θ_L	pitch-attitude lead term, deg
$\tau_1, \tau_2, \dots, \tau_5$	system time constants, sec
ϕ	roll attitude, positive right wing down, deg
ψ	yaw attitude, positive nose right, deg
$\Delta\psi$	aircraft heading relative to approach heading, deg
ω_n	undamped natural frequency, rad/sec

Subscripts:

b	bias value
c	commanded parameter
e	difference between actual value and reference value of parameter (i.e., error)
GS	groundspeed
GSE	groundspeed error
GSR	groundspeed reference
I	instrumentation sensor output
m	model parameter
N	refers to present computer cycle
N-1	refers to previous computer cycle
R	reference value

A dot over a symbol indicates a derivative with respect to time. A circumflex (^) denotes an estimator output.

EQUIPMENT

Airborne System

The automatic approach and landing concept was implemented on the CH-47B research helicopter shown in figure 1. This helicopter is a twin-turbine-engine, tandem-rotor vehicle with an allowable gross weight of 177 929 N (40 000 lb) and a maximum speed of approximately 160 knots. The operating weight during the flight tests reported herein was approximately 133 447 N (30 000 lb).

The helicopter was equipped with general-purpose digital and analog computing systems which could drive the pitch, roll, yaw, and/or collective flight-control channels through full-authority, parallel, electrohydraulic actuators. As noted in reference 3, the airborne hardware could be connected in a variety of ways to suit specific experiments. A simplified block diagram of the hardware configuration for the autoland experiments is shown in figure 2.

The digital computer is an 18-bit machine specifically designed for airborne applications. It has 16 384 words of magnetic core memory; 1024 words of solid-state, read-only memory; and 7 input/output (I/O) channels. Execution times for adds and subtracts are 4 μ sec; multiply and divide operations take 24 μ sec.

In the configuration shown in figure 2, four of the seven computer I/O channels were utilized. One channel was dedicated to the digital data link with the ground, two channels to control display units (pilots and system operators), and one channel to a digital interface unit (DIU).

The DIU provided the interface between the digital computer and the analog devices in the system. It can accept up to 30 analog inputs, plus 12 discretes, and can output the same number. The unit employs 12-bit converters and was operated under computer control; that is, all I/O transfers were initiated and controlled by the digital computer.

The analog computer is a general-purpose laboratory-type unit which has been ruggedized for the airborne installation. The computer employs solid-state computing components including operational amplifiers, integrator networks, and potentiometers. A variety of nonlinear devices such as comparators and diode function generators is also available but was not used in the present implementation.

The electronic control system (ECS) converts the electrical input signals from the analog computer to an electrohydraulic actuator position and hence a mechanical control-system input. A detailed description of the ECS and the actuator-clutch system is given in reference 3.

Ground-Based System

The position of the helicopter relative to a preselected touchdown point (the landing pad) was determined by a radar-laser tracking system. This system is part of the NASA Wallops Flight Center Aeronautical Research Radar Complex described in reference 4.

The helicopter was equipped with two retroreflector assemblies, one on each side of the fuselage, which served as the reference points for the laser tracking system (LTS). The location of the retroreflectors was such that at least one of the assemblies could always be "seen" by the LTS regardless of helicopter position, heading, or pitch and roll angle. In the event both retroreflectors were within the LTS coverage, the assembly producing the greater return was generally tracked. When the LTS switched from tracking one retroreflector to the other, an instantaneous change of up to 4.25 m (14 ft) could occur in the measured position. The transient resulting from this discontinuity was minimized by the onboard navigation algorithms.

The LTS range data and the azimuth and elevation angles from the radar pedestal were processed in a ground-based digital computer to derive the position of the helicopter in a runway referenced coordinate frame, with the origin at the touchdown point, as illustrated in figure 3. The Cartesian coordinate data were computed 10 times/sec during the present investigation and had an overall resolution of better than 0.305 m (1 ft).

It should be noted that all of the analyses, plots, and other calculations regarding position data reported herein are with respect to the estimated positions computed by the navigation algorithms. This, in turn, reflects the

position of the helicopter relative to the origin of the radar-laser derived data, as opposed to a fixed physical location on the runway.

Data Link

The radar-laser derived Cartesian coordinate position data were transmitted to the helicopter over a two-way digital data link referred to as the transponder data system (TDS) as indicated in figure 2. This system transmits a 10-bit digital data word with each radar ranging pulse. During the autoland tests described herein, the data rate on the uplink was approximately 51 frames/sec, a frame being one complete set of uplink data words. (Note however that the data were only computed 10 times/sec.)

Two 10-bit digital data words were used for each position transmission. That is, range (X), cross range (Y), and altitude (Z) were uplinked as 20-bit words. The paired words provided both the coverage and resolution needed for the autoland investigation being conducted.

The digital data link operated asynchronously from the digital computer program. Data transfers to the flight computer were accomplished through the use of an external interrupt which was generated by the TDS interface unit (TIU) whenever a complete frame of data was received from the ground. The interrupt service was under software control and was set up to transfer only one frame of data each main program cycle from the TIU to the computer. The significance of the various iteration rates associated with the data uplink will be addressed in a subsequent section of this report.

NAVIGATION

Overview

Ground-referenced position and velocity information was derived with an advanced digital version of the complementary filtering technique described in reference 5. As indicated in figure 4, the system provided output estimates of aircraft position and velocity in an Earth-referenced coordinate frame based on radar-laser position updates and onboard acceleration measurements. It also provided dead-reckoning position and velocity outputs, altitude and altitude-rate estimates, and wind estimates.

The first step in deriving the system outputs was to correct the onboard sensor inputs for known biases. Next, Earth-referenced accelerations were computed to provide high-frequency inputs to the complementary filters. Finally, these signals were blended with the telemetered radar-laser position signals to provide high-quality estimates of position and velocity.

The telemetered radar-laser position updates were continuously checked by a validation routine. Anytime the update signals failed the validation check, the system reverted to a dead-reckoning mode (that is, the position and velocity estimates were based entirely on onboard sensor outputs). If the

radar-laser update signals remained unusable for 20 sec, a discrete was generated which caused all the approach modes to be inhibited or automatically disengaged.

Signal Conditioning

Body-mounted accelerometers.— The body-mounted accelerometer outputs contained a significant amount of noise, mostly due to structural vibration at rotor frequencies of 1/rev and 3/rev. Before being sampled at 20 Hz and converted to digital signals, each of the body-mounted accelerometer signals was passed through a first-order analog filter with a time constant of 0.5 sec. Upon request from the system operator, the digital computer would automatically compute accelerometer bias values over a 30-sec period by using the technique shown in figure 5 for a_x . Similar computations were made for a_y and a_z using \ddot{y}_h and \ddot{z}_h , respectively. The accelerometer biasing operation was typically performed during preflight, or occasionally during a flight with the helicopter on the ground and stationary when the accelerations were known to be zero.

Vertical gyro.— The vertical gyro provided aircraft pitch- and roll-attitude information. The instrument maintained its vertical reference by automatically slaving to gravity at a rate of $2^\circ/\text{min}$ for both axes. In roll, there was an automatic cutout of the gravity slave mode if bank angle exceeded $\pm 9^\circ$. This prevented errors from accumulating in turns where the instrument would otherwise align itself to a false gravity. In pitch, there was no such automatic cutout, and it was found that during decelerating approaches, a pitch-attitude error would build up to a maximum of about 3° at the end of the deceleration. The attitude error resulted in an error in the computed horizontal acceleration which, in turn, caused an error of about 1.8 m/sec (6 ft/sec) in the velocity estimate. With the approach guidance-control gains used, the helicopter came to an initial hover approximately 15.2 m (50 ft) short of the pad. To correct this problem, open-loop compensation (as shown in fig. 6) was provided for pitch attitude in the digital computer.

Directional gyro.— The difference $\Delta\psi$ between magnetic heading, sensed by the directional gyro, and runway heading was used in the Euler transformation from body to Earth-referenced axes. Runway heading was manually entered into memory by the system operator with the control display unit shown in figure 7.

Euler Transformation Equations

The equations in this section were used to transform the body-mounted acceleration information into an Earth-referenced frame aligned with the runway. Note that the term a_z is positive upward and would normally be expected to have a value of approximately $1.0g$ in straight and level, unaccelerated flight. Since the normal sensor output of the accelerometer was biased by $-1.0g$ to have a nominal value of 0, $+1.0g$ was therefore added back to a_z within the digital computer before any transformation equations were processed. The equations are grouped so as to represent only one angular rotation at a

time. It was determined that this approach was very efficient in that it resulted in the minimum number of multiplications and divisions required for scaling. The transformation about the roll axis was performed first using the following equations:

$$\ddot{y}_h = a_y \cos \phi + a_z \sin \phi$$

$$a'_z = a_z \cos \phi - a_y \sin \phi$$

Next, the rotation about the pitch axis in a vertical plane was calculated using

$$\ddot{x}_h = a_x \cos \theta - a'_z \sin \theta$$

$$\ddot{z}_h = a'_z \cos \theta + a_x \sin \theta - g$$

Finally, the components of horizontal acceleration in the runway reference frame were determined:

$$\ddot{X} = \ddot{x}_h \cos \Delta\psi - \ddot{y}_h \sin \Delta\psi$$

$$\ddot{Y} = \ddot{y}_h \cos \Delta\psi + \ddot{x}_h \sin \Delta\psi$$

Complementary Filters

The complementary filter combines acceleration with position data to determine low-noise estimates of both velocity and position. Figure 8 is a block diagram representation of the complementary filter for X. There are similar complementary filters for Y, Z, and H. The part of the system drawn with solid lines (fig. 8) represents the high-frequency computation of velocity and position based on aircraft acceleration. Since acceleration is integrated directly to obtain these high-frequency components, there is no lag. The difference between the estimated position and the position measured by the tracking radar is fed back as a correction to both the velocity estimate and the acceleration input. (This feedback is indicated by the dashed lines in fig. 8.) Note that the velocity estimate is an output of an integrator, which attenuates the noise on the position input as well as that on the acceleration input.

The complementary filter gains which were used corresponded to a damping ratio of 0.707 and a natural frequency of $\omega_n = 0.4$ rad/sec, with a settling

time constant of 14 sec based on the time to settle within 2 percent of steady state. These gains were selected so that the time constant would be long enough that noise from the radar-derived position signal would be satisfactorily attenuated, but short enough that errors which would result from inaccuracies associated with the acceleration information would be kept small.

Validation Routine

A flow chart of the validation routine is shown in figure 9. This routine performed various checks to determine whether the radar position data contained certain obvious errors. An error code word was set to indicate either that the data were valid or, if not, what type of error had been detected.

The data transmission check verified that a new frame of data was received. Since data transfers to the digital computer only occurred when the entire transmitted data block was error free, data updates were frequently prohibited. Also, the radar-laser system had a failure mode wherein the same position data would be transmitted continuously for several seconds; therefore, a check was made to see that the position data were continuously changing (except when the aircraft had landed). To reject unreasonable values of position data, the position radar-laser data were required to be within a certain tolerance of the smoothed-position estimates. The tolerance values had to be small enough to prevent bad data from getting through, yet large enough to accommodate an expected level of noise and to permit the system to readily recover from dead reckoning. The tolerance values used were 27.4 m (90 ft) in X and Y and 12.2 m (40 ft) in Z.

The validation routine set a flag, CUPLFG, based on whether the data were valid. When CUPLFG = 1, all approach modes were enabled; when CUPLFG = 0, all approach modes were disengaged and/or disabled. The timing logic in setting CUPLFG is shown in figure 10.

Dead-Reckoning Modes

The flow chart in figure 11 indicates when dead reckoning was used and when the dead-reckoning computations were initialized. Note that when all approach modes are disabled (CUPLFG = 0), the navigation filters are forced to update using radar data even though the radar data may not be valid. This method was used to synchronize the navigation system to the radar-laser position.

The wind, of course, has a direct impact on the accuracy of the dead-reckoning estimates. Therefore, whenever the radar data were valid and air-speed was above 50 knots, the wind components were continuously estimated using the following expressions:

$$\hat{x}_w = V_h \cos (\Delta\psi + \beta \cos \phi) - \hat{x}$$

$$\hat{\dot{Y}}_w = V_h \sin (\Delta\psi + \beta \cos \phi) - \hat{\dot{Y}}$$

where $V_h = \sqrt{V^2 - \dot{H}^2}$, the horizontal components of airspeed.

If, during an approach, the radar data failed the validation tests and airspeed was above 50 knots, the last calculated values of the wind components were used in computing the dead-reckoning position estimates. The expressions were

$$\hat{\dot{X}}_d = V_h \cos (\Delta\psi + \beta \cos \phi) - \hat{\dot{X}}_w$$

$$\hat{\dot{Y}}_d = V_h \sin (\Delta\psi + \beta \cos \phi) - \hat{\dot{Y}}_w$$

The corresponding position estimates, \hat{X}_d and \hat{Y}_d , were obtained by integrating $\hat{\dot{X}}_d$ and $\hat{\dot{Y}}_d$.

Below an airspeed of 50 knots, the dead-reckoning estimates of horizontal position were obtained from the smoothed-position outputs of the complementary filters; that is,

$$\hat{X}_d = \hat{X}$$

$$\hat{Y}_d = \hat{Y}$$

This, in effect, eliminated the update mode altogether by providing zero-position-error feedback. (See fig. 8.) As such, the horizontal velocity and position estimates resulted from integrating acceleration information only, as in a pure inertial navigator. Airspeed was not used in the dead-reckoning computations below 50 knots due to limitations in the hardware and software configuration employed in the airspeed measurement.

For altitude dead reckoning, barometric altitude was substituted for radar-laser altitude when \hat{Z} was greater than 30.5 m (100 ft). (Below 30.5 m (100 ft), the barometric altitude sensor was not reliable because of ground effect.) A bias was added to the barometric altitude input to prevent a transient when switching to the dead-reckoning mode. In the dead-reckoning mode when \hat{Z} was below 30.5 m (100 ft), the dead-reckoning estimate for altitude was set equal to the smoothed-position output of the complementary filter, $Z_d = \hat{Z}$, thereby providing zero-position-error feedback in the complementary

filter. (See fig. 8.) In this mode, \hat{z} and \hat{z} were obtained by integrating \ddot{z} only, as in a pure inertial navigator.

GUIDANCE

Lateral Profile

The lateral profile used for the automatic approaches discussed in this report was a straight path 2440 m (8000 ft) in length. Capture logic was incorporated in the software which computed a flight path from the aircraft position at the time the automatic approach mode was selected up to the starting point of the path, that is, the 2440-m (8000 ft) range point. The logic insured that the aircraft captured the path with an appropriate heading (the approach heading with any required crosswind correction) at the correct initial speed and altitude.

The lateral path was stored in the computer by using the technique described in reference 6. The path was set up for a final approach heading of 0° , or due north. Alternate approach headings were obtained with a simple biasing routine in which the aircraft magnetic heading input to the computer was biased such that when the desired approach heading was being flown, the computer "thought" it was flying due north. It should be noted that all other magnetic heading input and output information to the computer was also biased to retain consistency.

Vertical Profile

The vertical profile, shown in figure 12, consisted of a constant-altitude segment of 244 m (800 ft), a 6° glide path starting at 2205-m (7236 ft) range and terminating at 15.2-m (50 ft) altitude and 30.5-m (100 ft) range, and a constant 15.2-m (50 ft) altitude segment to the hover point at zero range.

Although the vertical profile is stored in the computer with slope discontinuities at the junction of the straight-line segments, a smooth transition between segments is provided by a real-time subroutine which computes the instantaneous desired altitude on each computer cycle. The transition logic as described in reference 6 provides a smooth transition between segments; however, the reference path is undefined during the switchover period. This presents a problem in trying to display and/or record parameters such as glide-path deviation during the segment transition period.

Deceleration Profile

The deceleration profile employed in these tests was the constant-attitude profile described in reference 2. The profile was based on a nominal, no-wind, nose-up attitude 2° above the hover angle. The groundspeed profile, shown in figure 13, extended to 3048-m (10 000 ft) range and 136 knots. During an approach, the aircraft was commanded to fly a constant airspeed until the

deceleration (groundspeed) profile was intercepted. Transition logic was provided to insure a smooth switchover from airspeed to groundspeed control. The logic incorporated a "latch" to keep from cycling between airspeed and groundspeed control in the presence of gusts.

The technique for generating the reference velocity during the last series of flight tests differed considerably from the original one described in reference 6 which utilized a stored velocity profile. In the final version of the program, acceleration was stored in place of velocity as a function of distance to go. The groundspeed command (GSC) was computed in the real-time loop from the relationship

$$V_{GSC} = \sqrt{2A}$$

where A is the area under the acceleration curve between the touchdown point and the current position. The true simplicity of this approach can be illustrated by means of a sample calculation. Figure 13 includes the acceleration profile employed in the final version of the program. The entire profile was defined by four data points indicated by the circles in the figure. The in-line, real-time subroutine assumed zero acceleration at zero range; hence, only the remaining three data points were stored. Note also that path distance to go, rather than range, was used. This was done so that the deceleration technique would be applicable to curved approaches where range and path distance to go are not necessarily the same.

Computation of the pitch lead term and the reference velocity was as follows. The deceleration level associated with the current range was computed using interpolation. Assuming path distance to go is 1219 m (4000 ft), the deceleration level would then be 0.81 m/sec² (2.67 ft/sec²). The pitch lead term, in radians, was simply the deceleration level divided by gravity (in this example, Pitch lead = 0.083). The reference velocity was then computed from the area under the acceleration curve and, in this example, works out to be 78.4 knots.

The concept previously described offered two distinct advantages over the method described in reference 6. The reference velocity was a continuous function of range, and the pitch lead term was readily available. In the technique reported in reference 6, the lead term had to be obtained from the stored velocity profile by approximate differentiation. The overall computation time was approximately the same for both methods, but the profile storage requirements for the new technique were considerably less.

OUTER-LOOP CONTROL

General

The control laws were developed on the basis that at high speed (commanded groundspeeds greater than 40 knots), power (collective) would be used to control the vertical path, pitch would be used to control speed, and roll coupled

with yaw would be used to control the lateral path. At low speeds, power was still used to control the vertical path; yaw was used to control heading; and pitch and roll were used to fly the aircraft to a hover along the programmed speed profile and lateral path regardless of the direction in which the helicopter was heading.

The outputs of the outer-loop control laws were attitude commands in pitch and roll, a rate command in yaw, and a power command in the vertical degree of freedom.

The first step in processing the control laws was to determine which modes to use. Figure 14 is a simplified flow diagram showing the high-speed/low-speed decision logic. As indicated in the figure, the high-speed pitch and roll logic was always used in capturing the approach path. Once the path was captured, the high-speed logic remained in effect until the deceleration to a hover had been initiated and the commanded speed had dropped below 40 knots.

Signal Limiting

Signal limiting was used extensively throughout the outer-loop control logic. Two types of limiters were employed, a "hard" limiter and a "soft" limiter. The hard limiter was the classic type wherein the signal output was equal to the signal input for all inputs equal to or less than the limit value. For inputs greater than the limit value, the output equaled the limit value. In equation form:

$$E_O = E_i \quad (E_i \leq L)$$

$$E_O = L \quad (E_i > L)$$

The soft limiter, on the other hand, functioned according to the following equations:

$$E_O = E_i - \frac{E_i^2}{4L} \quad \left(\frac{E_i}{2} \leq L \right)$$

$$E_O = L \quad \left(\frac{E_i}{2} > L \right)$$

As indicated by the equations, the soft limiter avoided the sharp discontinuity between the input-output signal associated with hard limiters.

Pitch and Roll Commands

High-speed commands.— The high-speed pitch-command logic is shown in figure 15. During the constant airspeed portion of the approach, a speed

error signal was derived by taking the difference between the 80-knot initial approach speed and the output of a complementary filter (shown inside the dashed box in fig. 15). The filter utilized longitudinal acceleration in the horizontal plane (derived by the navigation algorithms) and measured airspeed. The feedback term, the difference between the measured and estimated airspeed, was soft limited to ± 5 knots and fed back on a gain K_3 of 0.125/sec, yielding an 8-sec time constant. The soft limit, illustrated in figure 15, limited the raw airspeed input and in effect produced a rate limit of 0.033g on that portion of the filter output due to the difference between the filtered output and the sensed airspeed. The speed error signal was multiplied by gain K_4 and the resulting signal hard limited to $\pm 10^\circ$. The output of the limiter was summed with lagged pitch attitude. Note that this is a positive feedback. When coupled with the negative feedback farther downstream (and discussed in a subsequent section), the effect was that of a "washout" network which prevented steady-state standoff errors. The time constant τ_1 of the first-order lag was the reciprocal of the longitudinal drag damping of the aircraft, and hence, approximated the velocity response time constant. The final pitch-attitude command was obtained by applying rate and magnitude limits to the resulting signal.

The switchover to the groundspeed reference was made when

$$(V_{GSE})(K_4) + \theta_L > 0$$

The logic that was employed incorporated a "latching" feature so that once the switchover to the groundspeed-deceleration mode was made, it would not switch back to the constant-airspeed mode. In the high-speed, groundspeed-deceleration mode, the reference groundspeed generated by the deceleration profile subroutine was compared with the estimated groundspeed from the navigation filter to form a groundspeed error signal. This term was multiplied by the outer-loop gain K_4 and summed with the pitch lead term also generated by the deceleration profile subroutine. The resulting, intermediate attitude command was sent to the $\pm 10^\circ$ attitude limit, as was the command generated by the constant-airspeed segment of the logic. Processing from this point forward was identical and utilized the same section of code.

The high-speed roll-command logic is shown in figure 16. It should be noted that the diagram has been simplified by excluding the capture logic and logic which pertains exclusively to flying curved paths in the lateral plane. The roll logic was based on matching the aircraft ground-track angle, computed by the navigation algorithms, against a track-angle command generated from the measured crosstrack error and the helicopter groundspeed. A soft limiter was employed to limit the track-angle command to a maximum of 45° . (It should be noted, however, that during a typical approach, the track-angle command never exceeded $\pm 3^\circ$.) The resulting track-angle error signal was converted to a lateral closure rate by multiplying it by groundspeed and then multiplying the result by K_6 , the velocity error gain. The signal was then rate limited and magnitude limited to produce the final high-speed roll command. As mentioned previously, yaw was coupled to roll in the high-speed mode. Yaw was in a turn-following mode such that whenever the helicopter

roll angle was nonzero, the heading would change in a conditioned fashion. When the helicopter rolled "wings" level, the existing heading was maintained. Considering this yaw mode in conjunction with the high-speed roll logic shown in figure 16, it can be seen that the helicopter will tend to establish the proper crab angle to stay on the lateral path (without a standoff) in the presence of a crosswind.

Low-speed commands.— As noted at the beginning of this section, once the commanded velocity dropped below 40 knots, pitch and roll were used to fly the aircraft to the hover point along the programmed speed profile and lateral path, regardless of the vehicle's heading. The logic utilized to accomplish this is shown in figure 17.

The first step was to derive the crosstrack rate command and the along-track rate command. The crosstrack rate command was calculated in the same manner in both the low-speed approach and hover modes. It was obtained by multiplying the crosstrack position (error) by gain K_7 and soft limiting the output to ± 20 knots maximum. The along-track rate command, on the other hand, depended on whether or not the vehicle had reached the hover. During the approach, the along-track command was equal to the groundspeed command generated in the deceleration profile subroutine. When the range to go was less than 7.6 m (25 ft), the logic was switched and latched to the hover mode. In this mode, the along-track rate command was calculated the same as the crosstrack rate command by using along-track position in lieu of crosstrack position.

In order to provide a smooth transition when switching modes, the longitudinal position gain of the deceleration profile near hover was matched to the hover gain K_7 . This was done by selecting the final deceleration level of the stored profile according to the relationship

$$\ddot{x} = (K_7)^2 x$$

The next step in computing the low-speed commands was to resolve the along-track and crosstrack rate commands into components relative to the vehicles longitudinal and lateral body axis. The equations used were

$$\dot{x}_{h,c} = \dot{x}_c \cos \Delta\psi + \dot{y}_c \sin \Delta\psi$$

$$\dot{y}_{h,c} = -\dot{x}_c \sin \Delta\psi + \dot{y}_c \cos \Delta\psi$$

As indicated in figure 17, the logic used to generate the pitch command and that used to generate the roll command were very similar. The time constants (τ_1 and τ_2) used in the first-order lags applied to the pitch- and roll-attitude feedbacks were matched to the vehicle's longitudinal and lateral drag damping characteristics.

Another feature incorporated into the logic to reduce touchdown dispersions involved increasing gains K_7 and K_8 once the aircraft reached the hover. This was done with a special subroutine which ramped up the gains to the hover value over an 8-sec period. The hover values employed represented a compromise between hover-accuracy requirements and the vehicle's pitch and roll activity from a pilot-passenger viewpoint. It should be noted that while increasing the position and velocity gains K_7 and K_8 , care was taken to make sure that K_8 led K_7 so as to not decrease the overall effective damping ratio during the ramp-up process.

Yaw Command

The high-speed and low-speed yaw-control logic is shown in figure 18. Considering the high-speed logic first, it can be seen that the yaw-rate command was composed of two components: one was a term based on the required nominal yaw rate calculated from the coordinated turn relationship

$$g \tan \phi = \dot{\psi} V$$

The other was based on nulling sideslip as derived from the body-mounted lateral accelerometer. Although the calculated sideslip angle was known to be in error due to the simplifying assumptions (such as side drag y_v/m being constant with speed) employed in the calculation, the error was immaterial since the goal was to null out any residual sideslip during turns.

The low-speed logic, which, it may be recalled, decoupled yaw entirely from the other degrees of freedom, was designed to simply point the aircraft in a desired direction specified by a heading reference value. This value was compared with the current compass heading to form an error signal. This signal was multiplied by the heading gain K_9 and hard limited to a maximum value of $\pm 5^\circ/\text{sec}$.

The final yaw-rate command was obtained by imposing rate and acceleration limits on the appropriate high- or low-speed command.

When the high-speed logic was active, the heading reference in the low-speed logic was continuously synchronized to the current heading. When the switch to the low-speed logic occurred, the synchronization stopped and the helicopter was commanded to maintain the heading which existed at the time of switchover.

A clearer understanding of the interplay between the roll and yaw modes may be gained by examining the sequence of events which would typically occur during a normal automatic approach in the presence of a crosswind. During the constant-airspeed portion using high-speed roll-yaw logic, the helicopter would automatically establish the proper crab angle required to fly down the approach center line. During the initial part of the deceleration when the high-speed roll-yaw logic was still in effect, the crab angle would gradually increase to compensate for the decrease in forward speed. When the low-speed logic switch-

over occurred, the crab angle ceased to change and the crosswind was compensated for by an appropriate roll (and/or pitch) input.

One of the features incorporated into the low-speed logic was that the pilot could insert a heading reference by way of his CDU (fig. 7) once the system switched to the low-speed mode. This feature was utilized to check out the low-speed pitch and roll logic. Specifically, during an otherwise normal automatic approach, the pilot inserted a reference heading 180° from the approach heading shortly after the logic switched to the low-speed mode. The helicopter began yawing while continuing down the approach path, coming to a hover over the center of the pad and heading 180° from the initial heading. Tests of this nature indicated that the low-speed pitch and roll logic functioned as designed.

Power Command

Figure 19 is a block diagram of the power-command logic. As stated earlier, this logic was employed throughout the entire approach; it operated in conjunction with both the high- and low-speed pitch, roll, and yaw logic.

As indicated in the figure, during an approach, altitude error was calculated by taking the difference between the estimated altitude from the navigation filter and the reference altitude generated by the vertical profile routine. This signal was multiplied by gain K_{10} to produce a vertical-velocity command proportional to altitude error. The resulting velocity signal was soft limited to ± 3.6 m/sec (± 700 ft/min) and summed with a lead term computed by the vertical profile routine.

The lead term is essentially the nominal vertical rate required to stay on the glide path at the current groundspeed. The signal at this point therefore is composed of the nominal component plus a component proportional to the altitude error. An asymmetrical hard limiter was then applied to the signal to produce the final vertical-velocity command.

In the land mode, the vertical-velocity command was generated by setting the reference altitude 6.1 m (20 ft) underground and forcing a descent rate proportional to K_{11} or the limit value of 1.5 m/sec (5 ft/sec), whichever was smaller in magnitude. It can be seen that this logic produced a commanded touchdown sink rate of 0.46 m/sec (1.5 ft/sec). The land mode could only be selected once the aircraft reached a hover and satisfied a set of criteria, as shown in figure 20. The pilot initiated the landing by pushing the land button on his control display unit shown in figure 7. Logic was incorporated in the software to prevent the pilot from selecting the land mode before the landing criteria was satisfied. An indication that the criteria were met and the land mode could be selected was provided by blinking the land light at a rate of about $1\frac{1}{2}$ times/sec.

The vertical-velocity-command signal calculated by either the approach logic or the land logic was then sent to a 0.1g rate limiter. The rate

limiter was actually incorporated for an alternate control mode which will not be discussed in this paper. It served no useful purpose in the present logic and, in fact, caused slight overshoots at glide-slope capture because it limited the commanded (and hence, actual) rate at which power was reduced. Simulator studies indicated that a glide-path overshoot of about 5.5 m (18 ft) occurred with the limiter in, although only a 1.8-m (6 ft) overshoot was encountered with it removed.

The vertical-velocity command was compared with the vertical-velocity estimate from the navigation filter to form a vertical-velocity error signal. Rate and magnitude limits were then applied to produce the final vertical-velocity-command signal.

INNER-LOOP CONTROL

Pitch and Roll Control

The pitch- and roll-attitude commands generated by the outer-loop control laws were sent to inner-loop control algorithms consisting of a second-order model and high-gain control loops to force the helicopter to follow the model response. The modified complementary filtering technique, described in reference 7, was employed in the model following loops of both pitch and roll degrees of freedom. The implementation employed in the present study differed somewhat from reference 7 in that an integrated attitude error closure was utilized. This is illustrated in figure 21 which represents both the pitch and roll inner-loop control laws.

A classical second-order filter served as the response model in both pitch and roll to generate acceleration, rate, and attitude commands corresponding to the outer-loop inputs. As indicated in figure 21, the pitch and roll model parameters were the same, namely: $K_{12} = 2/\text{sec}^2$ ($\omega_n = \sqrt{2}/\text{sec}$) and $K_{13} = 2.12/\text{sec}$ ($2\zeta\omega_n$). This yielded a damping ratio ζ of approximately 0.75.

The model following-loop structure and the rate error gain K_{14} , the attitude error gain K_{15} , and the integrated attitude error gain K_{16} were also the same for pitch and roll. The differences between the two channels were in the gains employed in the complementary filter. As indicated in the figure, the plant (unaugmented helicopter) was modeled as a first-order response. The time constant of the plant τ_3 was assumed to be 1.0 sec in pitch and 2.0 sec in roll. Although these levels were lower than the reciprocals of the respective angular-velocity damping values presented in reference 8, the choice is not critical, particularly at the short complementary-filter time constants τ_4 employed (i.e., 0.1 sec in pitch and 0.2 sec in roll).

A comprehensive discussion of the effects of the plant model characteristics and the filter time constant on the rate estimate is given in reference 7.

Yaw Control

Whereas the outer-loop logic generated attitude commands in pitch and roll, a rate command was generated in yaw. The inner-loop logic therefore utilized a first-order model as shown in figure 22. The inputs to the model-following loops were the model's acceleration and rate response computed from the outer-loop input.

The modified complementary filtering technique (ref. 7) was used to estimate the helicopter yaw rate in the feedback loop. However, unlike pitch and roll, an acceleration model was used for the simplified plant model. As indicated in reference 8, the vehicle yaw-rate damping is near zero throughout the flight envelope. As indicated in the figure, the complementary-filter time constant τ_5 was 0.1 sec.

The model-following loops included a rate error term with gain K_{19} and an integrated rate error term with gain K_{20} . The model angular-acceleration term was used as a lead term.

Collective Control

As noted earlier in this paper, model following was not employed in the vertical degree of freedom. The power command generated by the outer-loop logic was sent to the control system by using proportional plus integral gain, as illustrated in figure 23. The gains in this case (K_{21} and K_{22}) are expressed in terms of centimeters (inches) of collective per meter (feet) or meter per second (feet per second) since the aircraft vertical acceleration per centimeter (inch) of control varies considerably with flight condition. Without the model-following technique, the overall closed-loop system gain is therefore varying.

IMPLEMENTATION

Up to now, the control algorithms have been discussed without regard to the type of implementation utilized, that is, whether the implementation was digital or analog. In the present study, the outer-loop control laws, the collective control inner-loop, the pitch, roll, and yaw model response, the model lead terms, and the integrated altitude-error terms (in pitch and roll) were calculated in the digital computer. Only the high-gain feedback loops, including the modified complementary filter, were programmed on the analog computer.

The digital flight-system software was organized as a set of subroutines, called in sequence every 50 msec by a master routine. The organization was similar to that reported in reference 6 except that a single-cycle, real-time loop was employed as opposed to the split-cycle loop reported in the reference. Figure 24 illustrates the ordering of the primary events in the real-time loop.

As indicated in the figure, the first step in the real-time loop was to service the DIU. Execution of the main program was suspended during the

servicing process which took approximately 2 msec. The next step was to calculate all the integrals used in the program. The integration routine was based on the following equation:

$$Y_N = Y_{N-1} + T\dot{Y}_{N-1}$$

where Y_N is the integral calculated during the present cycle, Y_{N-1} is the integral calculated during the previous cycle, \dot{Y}_{N-1} is the integrand calculated during the previous cycle, and T is the sample period (0.05 sec). Truncation errors normally associated with integer calculations of this type were minimized by carrying the remainder from the \dot{Y}_{N-1} calculation of the previous cycle over to the current cycle and adding it to the integrand of the current cycle.

Following the integration routine, the TDS inputs (uplinked position information) received during the latter half of the previous cycle and the DIU inputs (sensor information) received at the beginning of the current cycle were processed. This involved scaling, biasing, and in some instances forming sines, cosines, and/or angles with respect to selected sensor inputs. Execution of the input processing subroutines completed the preparations for solving the navigation, guidance, and control algorithms.

Following the navigation, guidance, and control computations, the DIU output buffers were loaded and the real-time loop exited. The background loop in the autoland software was essentially a wait loop used until the next real-time cycle was due.

The scaling used in the autoland software routines is shown in table I. Intermediate calculations within the routines were structured so as to retain as much resolution as possible.

SYSTEM PERFORMANCE

Approach Data

The performance of the system will be illustrated by examining the approach tracks and touchdowns of 21 automatic landings. The data were obtained during two separate flight test series. The first series, composed of 14 automatic approaches, used a slightly different altitude profile than described in a previous section, an earlier set of gains, and the original deceleration-profile generation technique. Specifically, the 6° glide path during the first test series terminated over the center of the pad instead of at 30.5-m (100 ft) range, as shown in figure 12 for the second series of tests. During the first series of tests, the altitude error gain (K_{10} in fig. 19) was lower (0.17 instead of 0.4) and the integral-rate error gain (K_{21} in fig. 23) was higher (0.032 instead of 0.016). In addition, the pitch and roll model-following loops did not include integral attitude error closures (i.e., K_{16} in fig. 21 was equal to zero) during the first series of tests. Because of these differences, the two series of approaches were analyzed separately and the results will be presented accordingly.

Although flight data from decelerating approaches to a hover (or landing) have been reported using other aircraft (ref. 9) or hardware and software configurations (ref. 10), comparisons with the present results are not considered appropriate. In reference 9, a U.S. Army helicopter was used to fly hands-off, autopilot approaches to a hover by using guidance from a scanning-beam landing system. The trajectory employed was very similar to that of the study reported herein but only sample data were presented; there were not enough data for a meaningful comparison with the current results. In reference 10, on the other hand, the data are appropriate, but the trajectories flown were so dissimilar that any comparisons could be misleading. It should be noted that although the study reported in reference 10 utilized the same helicopter as the present study, the navigation, guidance, and control algorithms were totally different.

Profile Tracking Performance

Figure 25 is a composite plot of the approach tracks from the first test series of 14 automatic landings. The figure shows groundspeed, cross range, and altitude as a function of range. The surface wind and approach heading for each of the approaches plotted is given in table II.

Figure 26 is a similar composite plot showing the tracks from the second test series of 7 automatic approaches. The wind data associated with these approaches are given in table III.

The programmed groundspeed deceleration profile is shown by the dashed line in figures 25 and 26 from 1600-m (5000 ft) to 0-m (0 ft) range. As noted in a previous section, the aircraft was commanded to fly a constant airspeed of 80 knots until intercepting the deceleration profile. The presence of head winds (and in one instance, a tail wind) at altitude is apparent in both figures by virtue of the recorded groundspeed at 80 knots airspeed. The effect of the winds, of course, is to simply alter the range at which the deceleration profile is intercepted. Once on the groundspeed deceleration profile, the effects of winds are counteracted by the pitch-control loop.

The performance of the pitch-control loop was examined by performing a statistical analysis on the groundspeed error from the deceleration-profile intercept point to the hover. The results are given in the following table:

	First series	Second series
Mean, knots	-0.2	0.2
Standard deviation, knots	1.4	0.8
Maximum positive error, knots	4.5 (slow)	1.7
Maximum negative error, knots	-5.7 (fast)	-3.1

These data indicate similar performance during both series of tests. This is consistent with the fact that the algorithms and gains employed in both series of tests were essentially the same.

Specifications, of course, do not currently exist for helicopter automatic landing systems. There is, however, a specification for system performance of conventional aircraft for Category IIIa landing weather minima (ref. 11). Although not directly applicable to the present results, it does offer a basis for comparison. The specification states, in part, that the system should automatically adjust throttles to maintain airplane speed to within ± 5 knots of stabilized programmed airspeed. As indicated by the results shown in the previous table, the system described herein maintained groundspeed within ± 5 knots of a varying programmed groundspeed (the deceleration profile).

It should be noted that the groundspeed tracking performance previously described was achieved with relatively low outer-loop gains. This resulted in achieving good accuracy while maintaining very good ride qualities.

The cross-range tracking performance was analyzed from 3048-m (10 000 ft) range to touchdown for the first series and from glide-slope intercept to hover for the second test series. The results of the analysis were as follows:

	First series	Second series
Mean, m (ft)	1.5 (4.8)	2.0 (6.6)
Standard deviation, m (ft)	2.9 (9.5)	2.4 (8.0)
Maximum positive error, m (ft)	11.1 (36.5)	9.9 (32.5)
Maximum negative error, m (ft)	-10.8 (-35.5)	-8.8 (-28.8)

Here again, similar performance was obtained during both series of tests. This was also anticipated since the modification to the model-following loop was considered to be a higher order refinement.

The data indicate that the tracking was both accurate and consistent. The aircraft motions associated with these approaches were characterized by smooth, well-damped, positive corrections. The tracking is probably more accurate than that required for most applications. However, there was no need to decrease the gains (i.e., soften the ride) since the associated ride qualities were excellent.

A comparison between the cross-range tracking performance and the localizer performance criteria of reference 11 indicates that the performance is better than that required by conventional aircraft criteria. The comparison to conventional aircraft criteria is, of course, subject to considerable interpretation. In the present context, the comparison is only being offered as an observation.

The performance of the system in the vertical degree of freedom was examined next. It may be recalled that the vertical loop employed different gains during the two series of tests and slightly different altitude profiles. With this in mind, an analysis of the altitude error was performed in the interval following glide-path capture to the beginning of the vertical descent to touchdown to yield the following results:

	First series	Second series
Mean, m (ft)	-1.0 (-3.3)	0.7 (2.4)
Standard deviation, m (ft)	2.2 (7.2)	2.3 (7.5)
Maximum positive error, m (ft)	7.2 (23.7)	8.1 (26.5)
Maximum negative error, m (ft)	-7.5 (-24.7)	-4.4 (-14.5)

where a positive error indicates the helicopter was above the glide path.

Here again the results are similar, which indicates that the gain adjustments had a minor effect on the tracking errors of the total system. Typically, the aircraft went above the glide path at the beginning of the deceleration. The maximum negative error usually occurred in the 152- to 244-m (500 to 800 ft) range where the power required was increasing noticeably. The performance prior to glide-slope capture was not analyzed but should be as good as or better than the glide-path performance since the control logic is the same and the reference altitude is constant as opposed to changing.

Whether the system performance illustrated in the previous sections is adequate depends on the specific task at hand. In the present investigation, the task was to fly preprogrammed (stored) velocity, lateral, and altitude profiles to a stabilized 15.2-m (50 ft) hover. There was an implied goal to accomplish this task with reasonable tracking accuracy and without sacrificing ride qualities. The results indicate that this goal was achieved. Specifically, the flight tests demonstrated that the algorithms described in this report can produce good tracking accuracy in conjunction with good ride qualities on a consistent basis.

Touchdown Performance

The touchdown performance during the first series of tests is illustrated by figure 27 which shows the position of the aircraft reference point (approximately the center of gravity) at touchdown. As indicated in the figure, the touchdowns were off both laterally and longitudinally, in some cases as much as 9.1 m (30 ft). An analysis of the system indicated that resolution was being "lost" in the pitch- and roll-control computations due to truncation within the digital computer calculations. The program was subsequently rescaled by increasing the low-speed velocity scale factors, as indicated in table I.

In order to further improve the touchdown performance, the outer-loop position and velocity gains were also modified. During the first series of flight tests, the same gains were employed for both approach and landing. During the second series of tests, the gains were increased for hover and landing, as explained in a previous section.

The effect of these modifications is illustrated in figure 28, which includes a sketch of the helicopter, shown to scale, and aligned with the approach (runway) heading. As indicated by the figure, the touchdown dispersion was very small, the farthest touchdown being less than 3.6 m (12 ft)

measured radially from the center of the pad. For this set of data, the mean was calculated to be approximately 0.9 m (3 ft) forward and 0.6 m (2 ft) right of center. An examination of the helicopter velocity prior to touchdown showed that, in all but two cases, the aircraft was moving toward the center of the pad at touchdown. In one of the two exceptions, the aircraft was very near the center of the pad, moving away at less than 2 knots. In the other case, the helicopter was approximately 3 m (10 ft) forward and still moving forward but at less than 1 knot. For this case, however, the recorded surface winds were gusting up to 28 knots.

Despite using higher gains, the aircraft appeared very stable in a hover under all the wind conditions encountered. Both analytical and flight experiments indicated that even higher gains were usable if required. Considering the performance obtained, however, there appeared to be no reason to increase the gains any further.

CONCLUDING REMARKS

This report has described the navigation, guidance, and control algorithms used to perform automatic approach and landings with a helicopter. The algorithms were implemented in a digital computer (with some feedback loops in an analog computer) and represented a mature concept which had been developed while performing hundreds of approaches over a 10-yr period.

The performance provided by the algorithms has been illustrated by the capability of the vehicle to follow stored lateral, vertical, and velocity profiles to a landing. A statistical analysis of the tracking errors indicates the performance is both consistent and accurate. In general, the performance is better than the minimum required of automatic landing systems in conventional aircraft. (This comparison, of course, is subject to considerable interpretation.)

The tracking performance was achieved in conjunction with good ride qualities. The outer-loop response characteristics were such that corrections were smooth without any apparent oscillations.

Langley Research Center
National Aeronautics and Space Administration
Hampton, VA 23665
February 28, 1980

REFERENCES

1. Garren, John F., Jr.; Kelly, James R.; and Sommer, Robert W.: VTOL Flight Investigation To Develop a Decelerating Instrument Approach Capability. [Preprint] 690693, Soc. Automot. Eng., Oct. 1969.
2. Kelly, James R.; Niessen, Frank R.; Thibodeaux, Jerry J.; Yenni, Kenneth R.; and Garren, John F., Jr.: Flight Investigation of Manual and Automatic VTOL Decelerating Instrument Approaches and Landings. NASA TN D-7524, 1974.
3. Kelly, James R.; Niessen, Frank R.; Garren, John F., Jr.; and Abbott, Terence S.: Description of the VTOL Approach and Landing Technology (VALT) CH-47 Research System. NASA TP-1436, 1979.
4. Instrumentation Handbook - Volume III. Data Systems and Facilities, Wallops Flight Center, Apr. 1979.
5. Niessen, Frank R.: A Low-Cost Inertial Smoothing System for Landing Approach Guidance. NASA TN D-7271, 1973.
6. McConnell, Walter J., Jr.; Skutecki, Edmund R.; and Calzado, Alfonso J.: Development of the NASA VALT Digital Navigation System. NASA CR-144894 [1975].
7. Garren, John F., Jr.; Niessen, Frank R.; Abbott, Terence S.; and Yenni, Kenneth R.: Application of a Modified Complementary Filtering Technique for Increased Aircraft Control System Frequency Bandwidth in High Vibration Environment. NASA TM X-74004, 1977.
8. Ostroff, Aaron J.; Downing, David R.; and Rood, William J.: A Technique Using a Nonlinear Helicopter Model for Determining Trims and Derivatives. NASA TN D-8159, 1976.
9. Demko, P. S.; and Boschma, J. H.: Advances in Decelerating Steep Approach and Landing for Helicopter Instrument Approaches. Preprint No. 79-16, Proceedings of the 35th Annual National Forum, American Helicopter Soc., May 1979.
10. Downing, D. R.; Bryant, W. H.; and Ostroff, A. J.: Flight Test of a VTOL Digital Autoland System Along Complex Trajectories. AIAA Paper 79-1703, Aug. 1979.
11. Criteria for Approval of Category IIIa Landing Weather Minima. AC No. 120-28B, FAA, Dec. 1, 1977.

TABLE I.- PARAMETER SCALE FACTORS

Parameter	Bits/unit ^a
Angles	500/deg
Angular rates	500/deg/sec
Linear accelerations	420/m/sec ² (128/ft/sec ²)
High-speed velocities (horizontal plane)	26/m/sec (8/ft/sec)
Low-speed velocities (horizontal plane)	^b 105/m/sec (32/ft/sec)
Vertical velocities	105/m/sec (32/ft/sec)
Altitude	52/m (16/ft)
Horizontal positions	13/m (4/ft)
Control positions	394/cm (1000/in.)

^aThe computer was scaled with the U.S. Customary Units; hence, the U.S. Units are exact. The SI scale factors are accurate to within 1 bit.

^bDuring the first test series, the scale factor was 26/m/sec (8/ft/sec).

TABLE II.- SURFACE WIND CONDITIONS FOR FIRST TEST SERIES

Approach	Runway heading, deg	Wind direction, deg	Wind magnitude, knots
1	280	260	6 to 12
2	280	330	10 to 18
3	280	310	7 to 18
4	350	310	4 to 16
a5	350	290	4 to 16
6	280	360	3 to 5
7	280	290	2 to 5
8	280	260	4 to 8
9	280	260	4 to 10
b10	280	360	3 to 7
11	100	40	10 to 14
c12	100	60	10 to 14
13	100	60	10 to 16
14	100	60	7 to 12

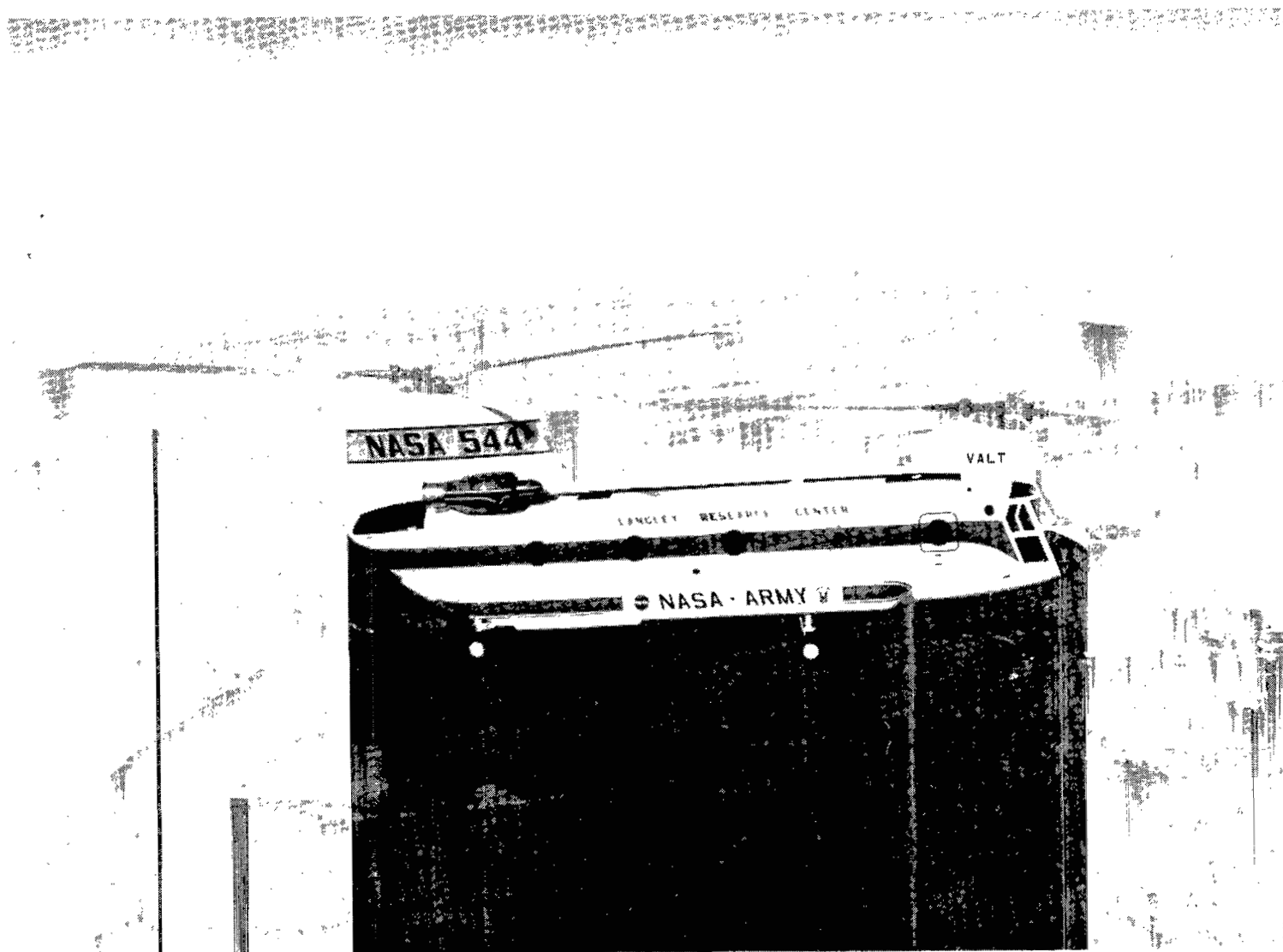
^aLeft turn to 260° selected in low-speed mode.

^bRight turn to 100° selected in low-speed mode.

^cLeft turn to 280° selected in low-speed mode.

TABLE III.- SURFACE WIND CONDITIONS FOR SECOND TEST SERIES

Approach	Runway heading, deg	Wind direction, deg	Wind magnitude, knots
1	280	300	5 to 14
2	280	270	6 to 12
3	170	150	7 to 12
4	170	190	10 to 17
5	350	330	13 to 28
6	350	330	4 to 10
7	350	350	3 to 4



L-74-8037

Figure 1.- CH-47B research helicopter.

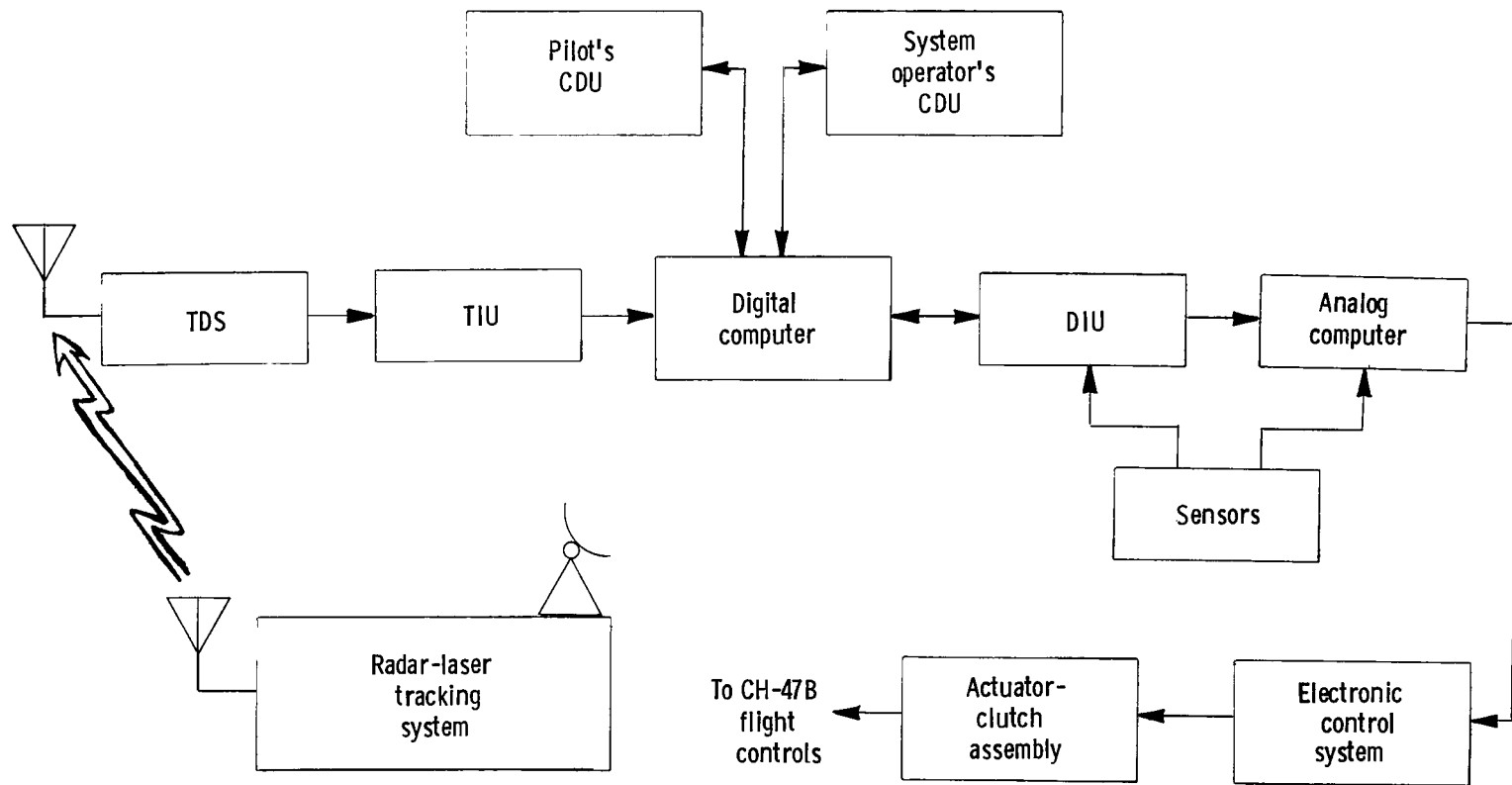


Figure 2.- Hardware configuration.

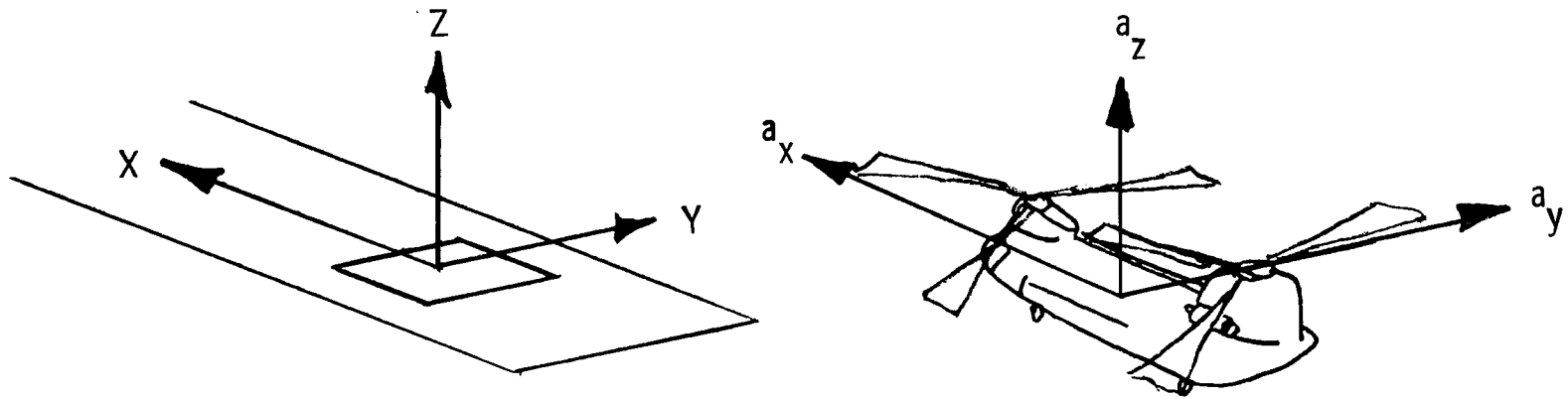


Figure 3.- Aircraft and runway reference coordinate frames.

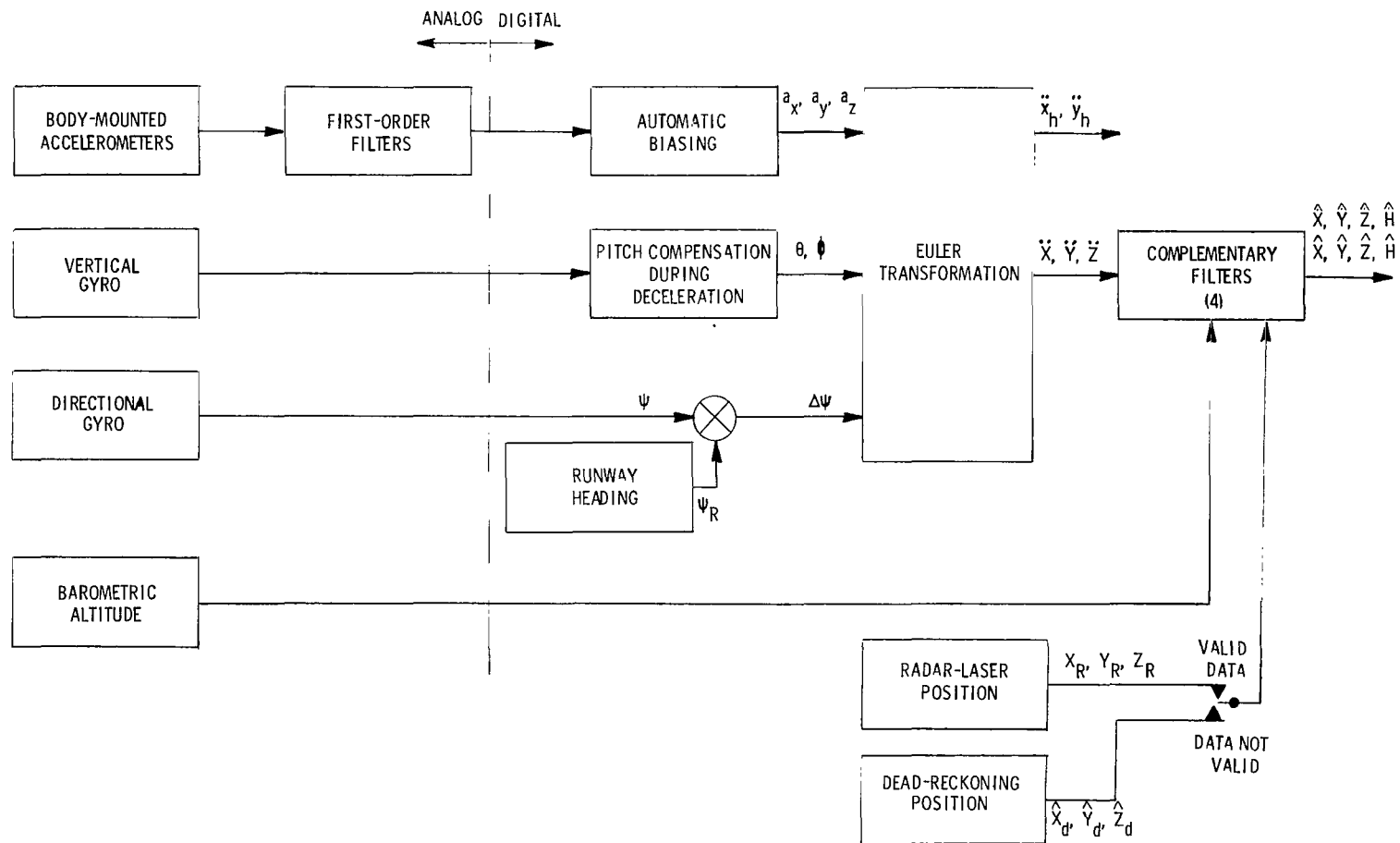


Figure 4.- Navigation system.

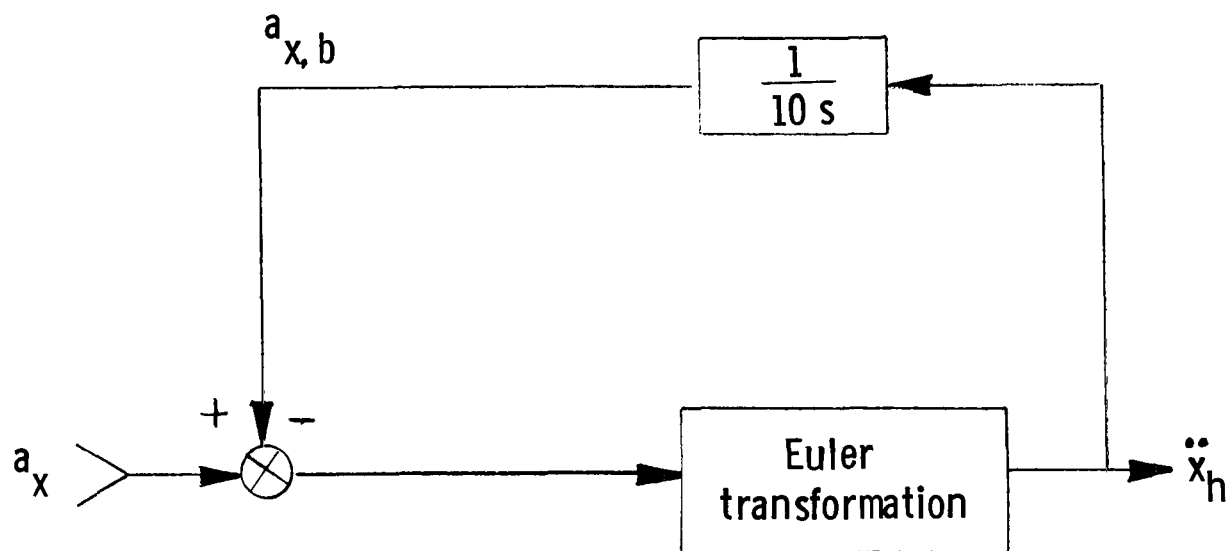


Figure 5.- Accelerometer biasing.

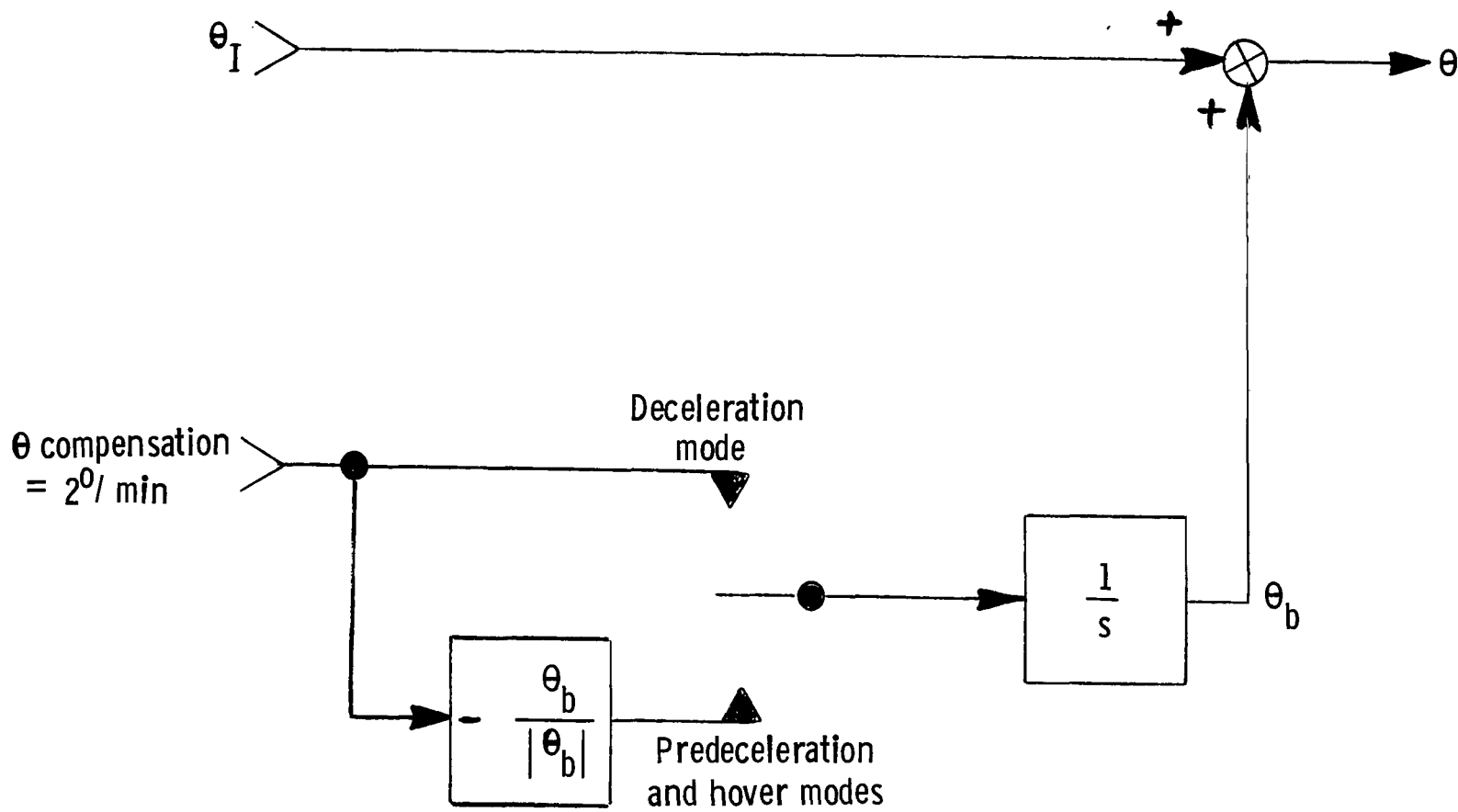


Figure 6.- Pitch-attitude gyro compensation.

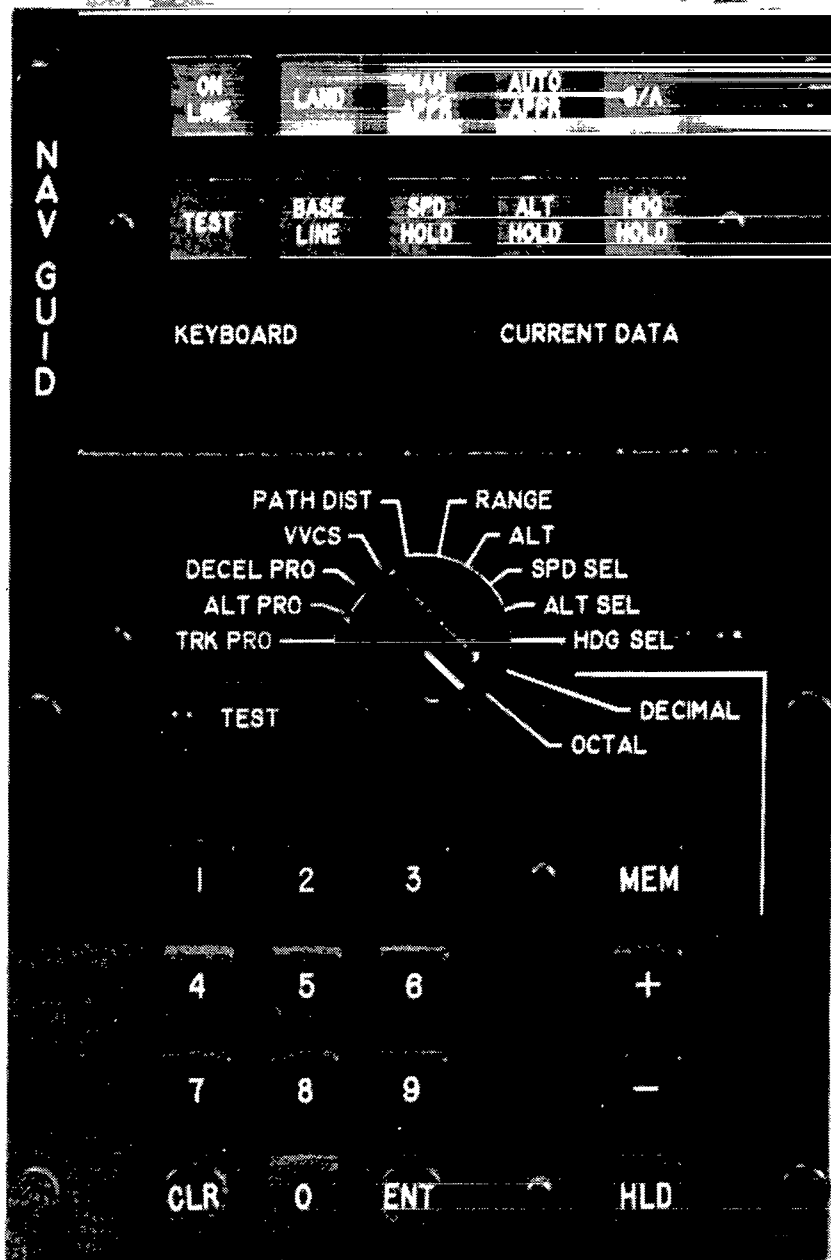


Figure 7.- Control display unit.

L-78-318

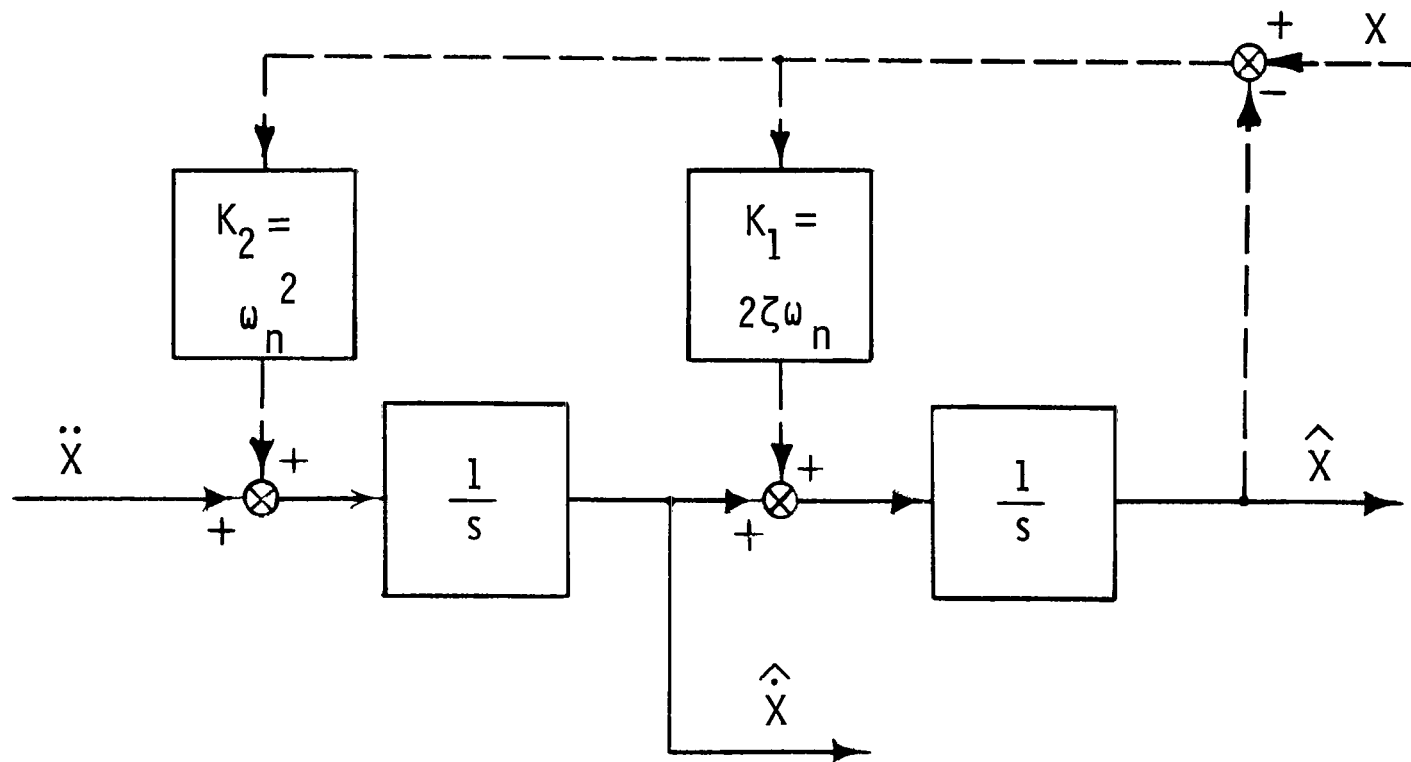


Figure 8.- Complementary filter for X-position estimate.

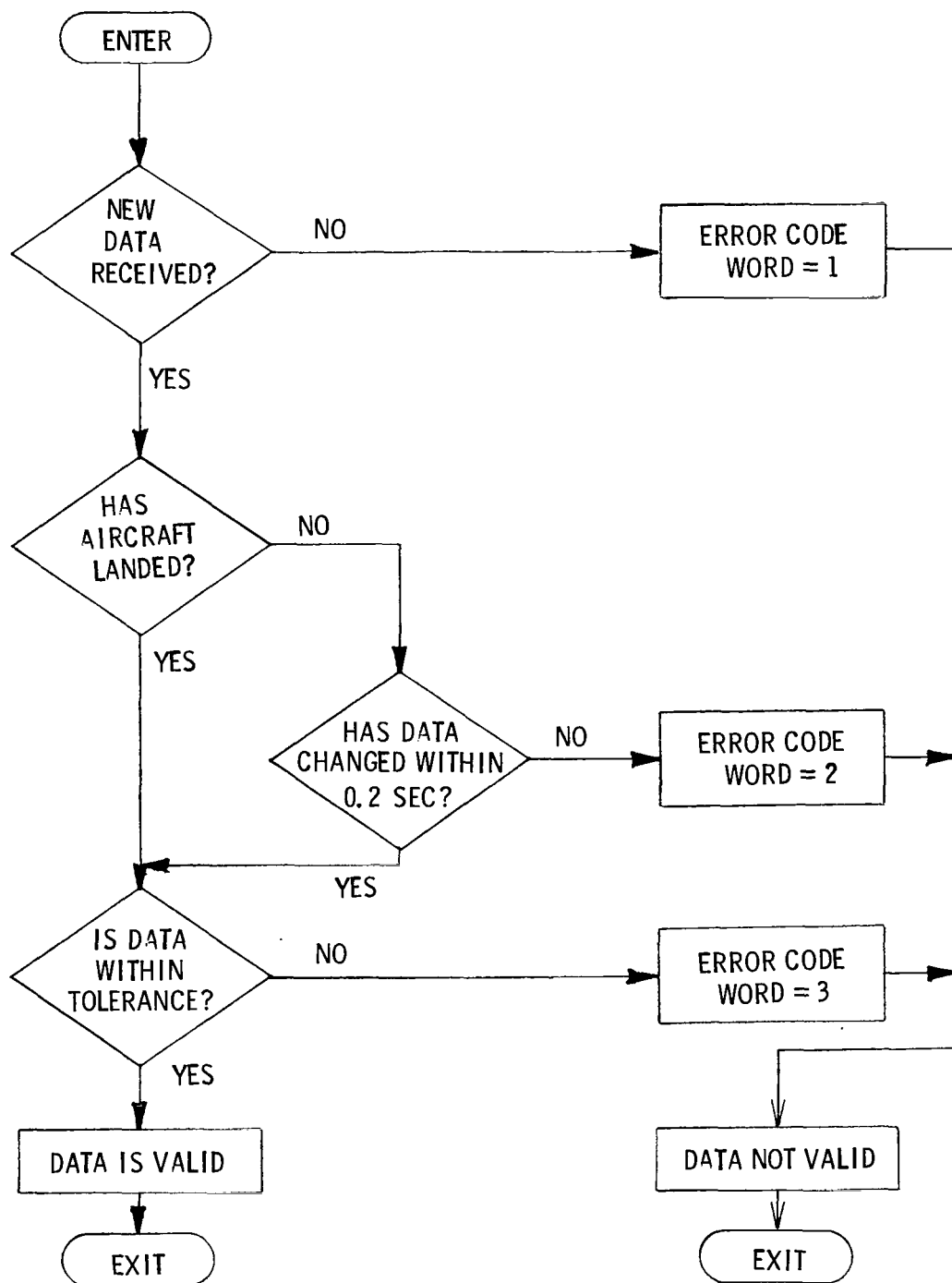


Figure 9.- Validation routine flow chart.

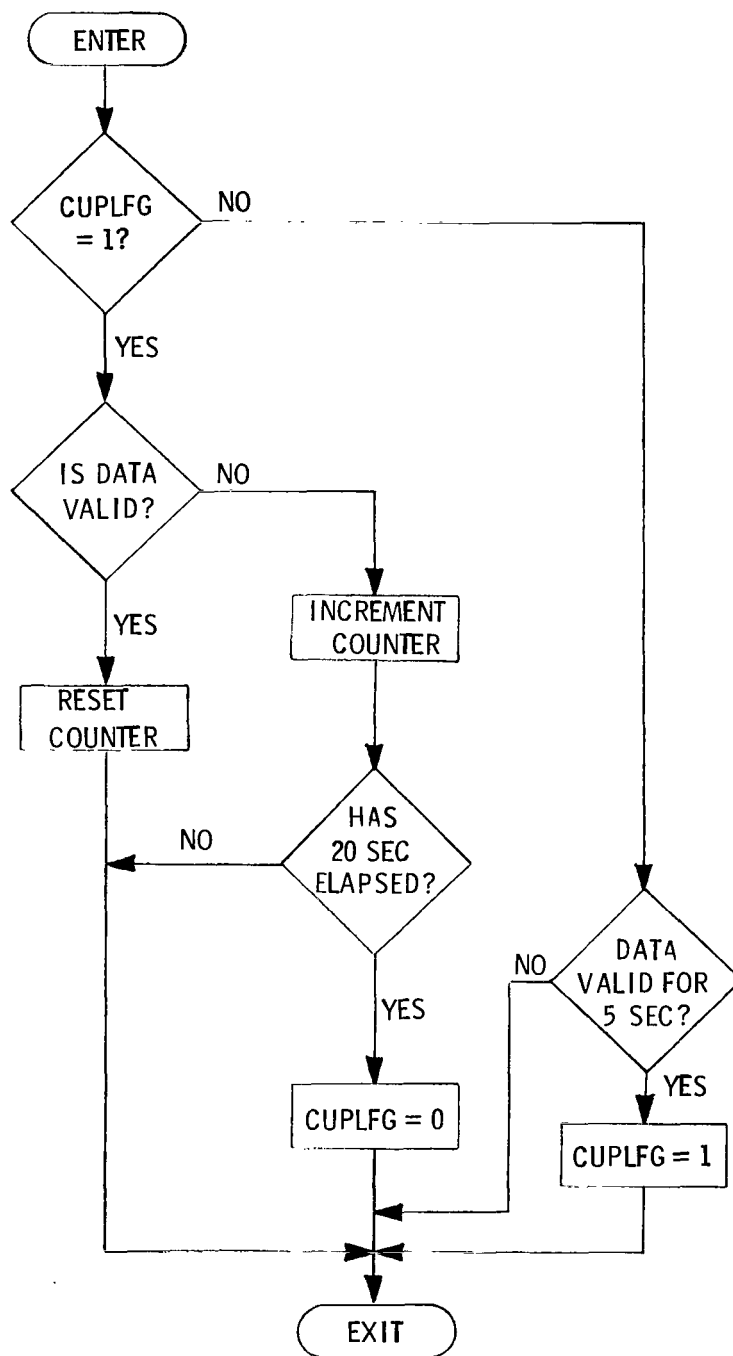


Figure 10.- CUPLFG logic flow chart.

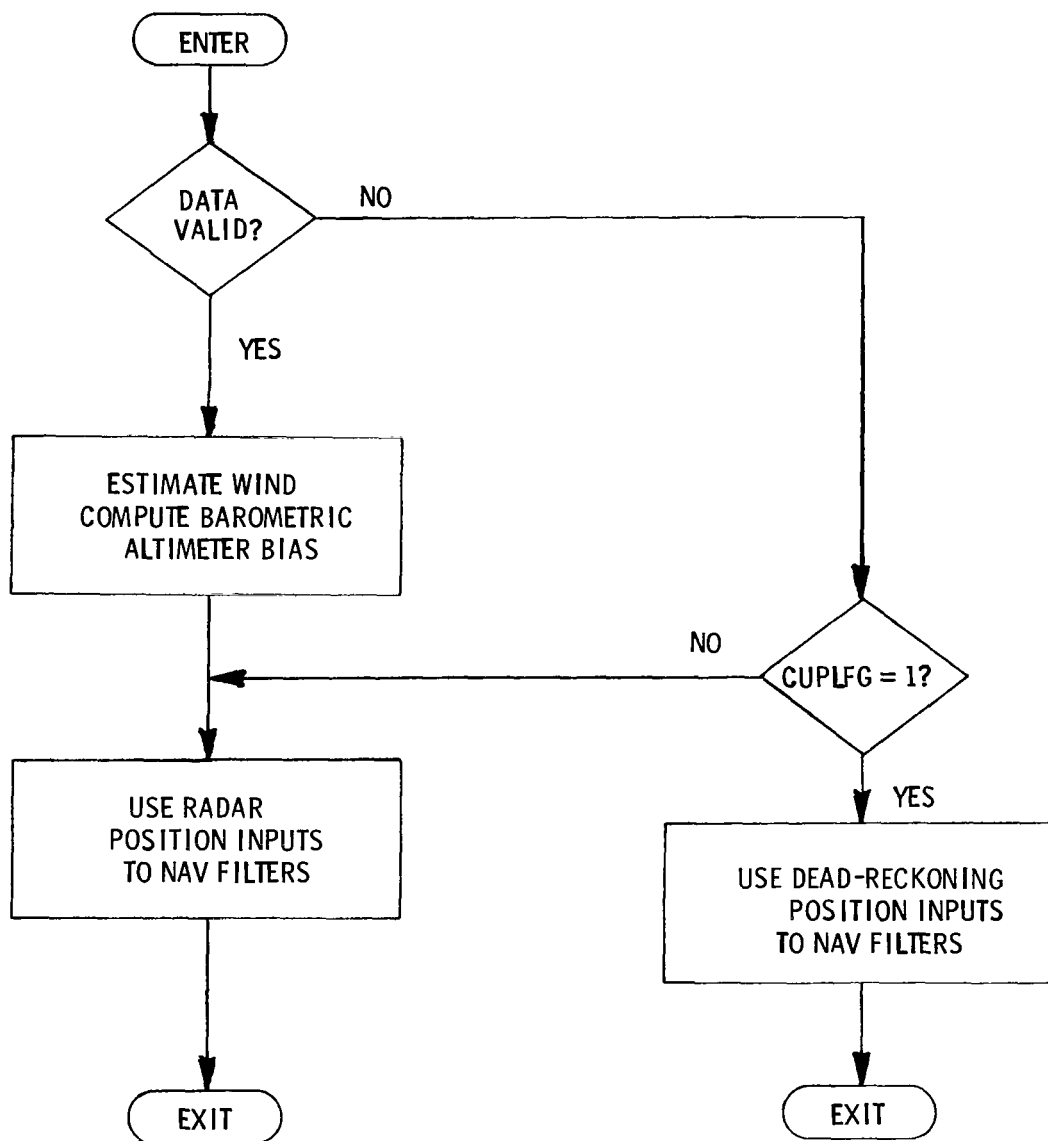


Figure 11.- Dead-reckoning logic flow chart.

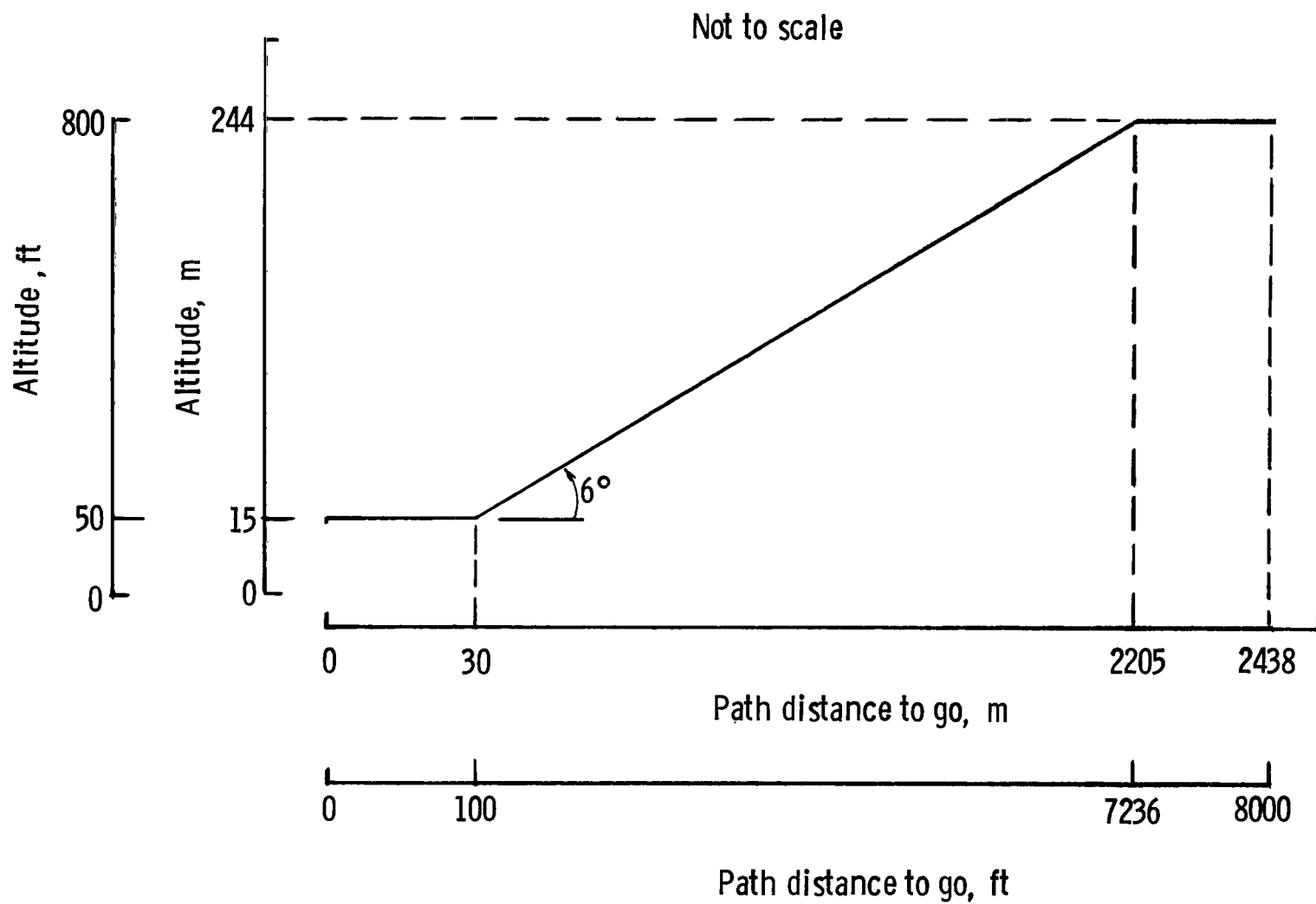


Figure 12.- Vertical profile.

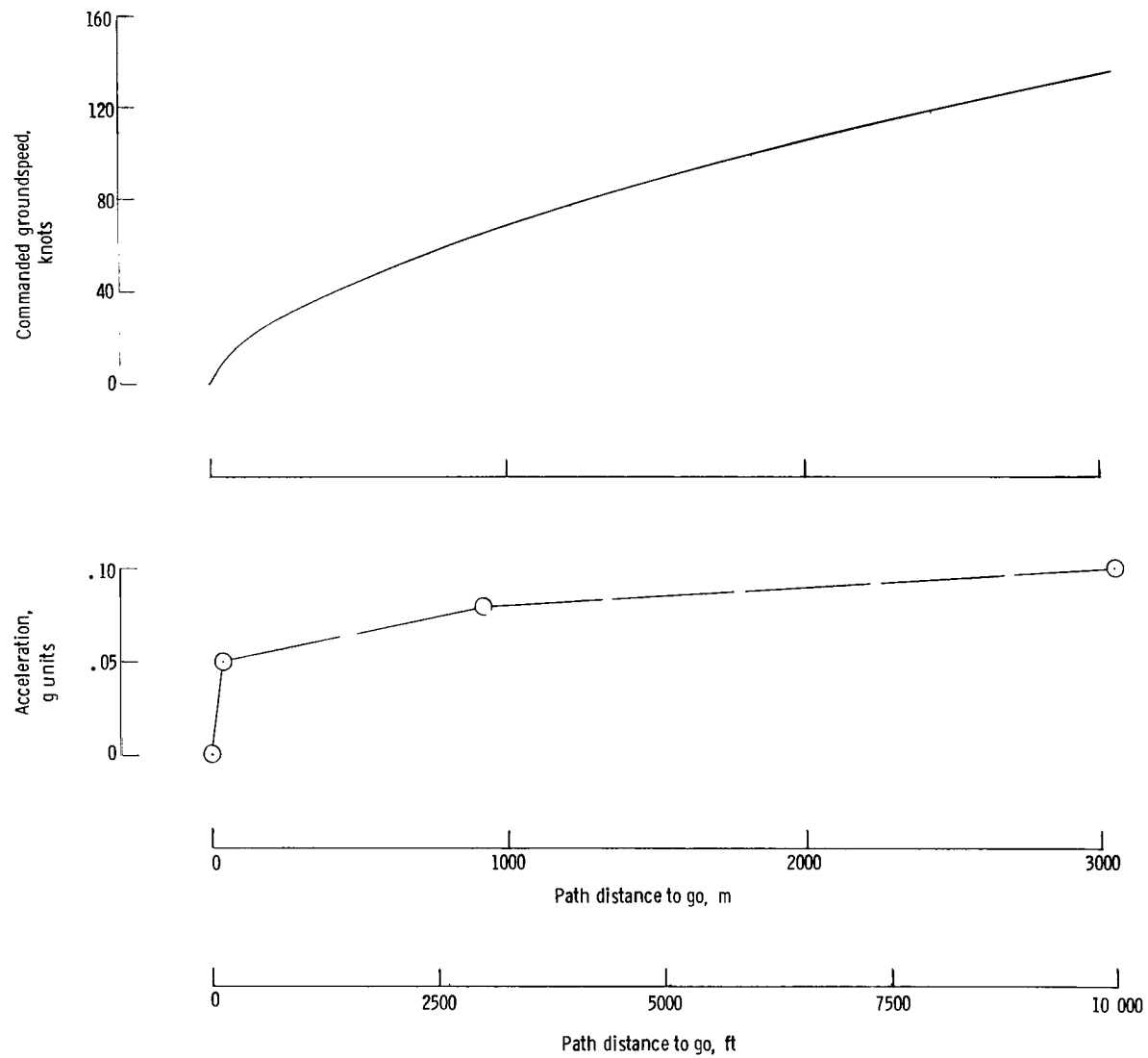


Figure 13.- Deceleration profile.

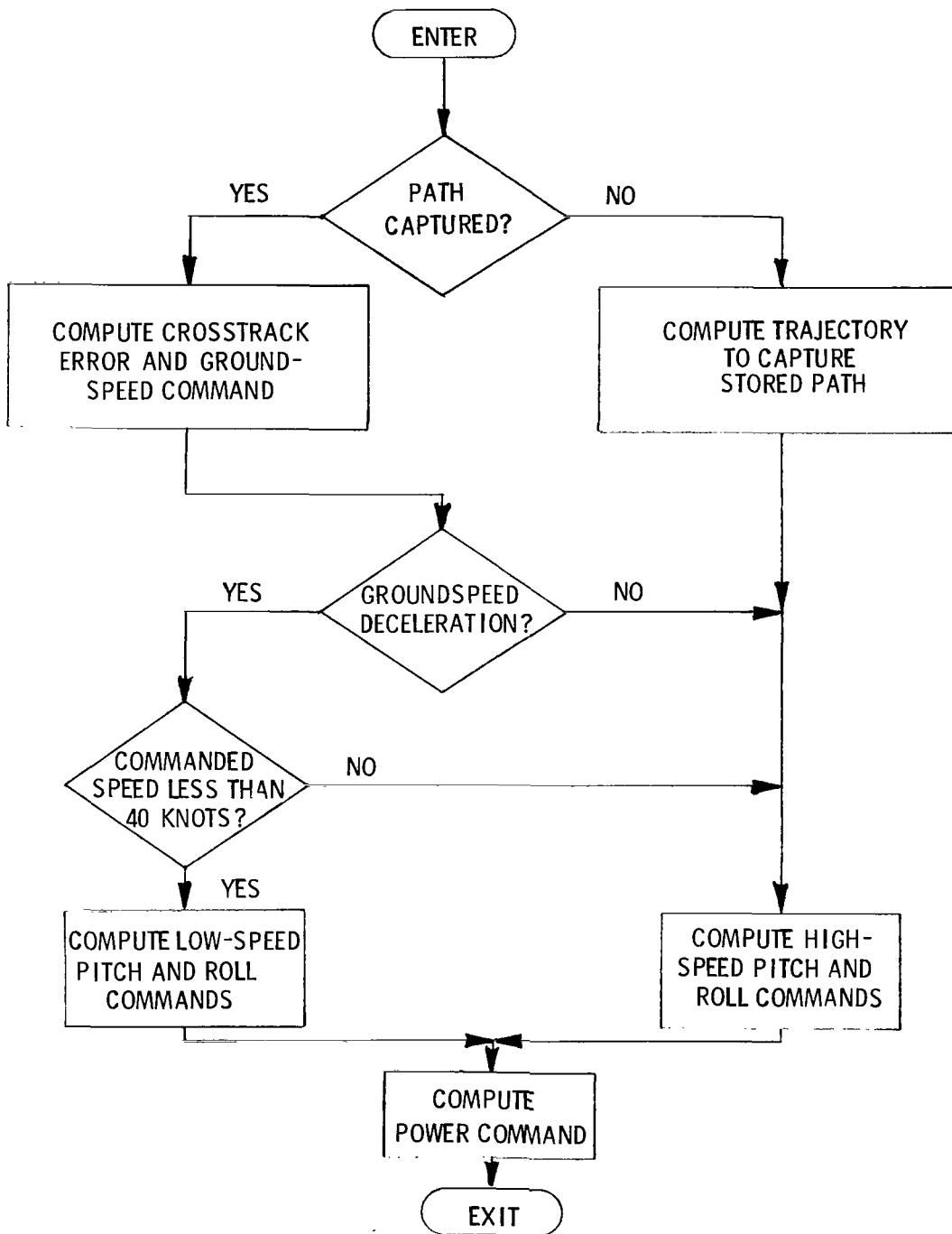


Figure 14.- Control-mode decision logic flow chart.

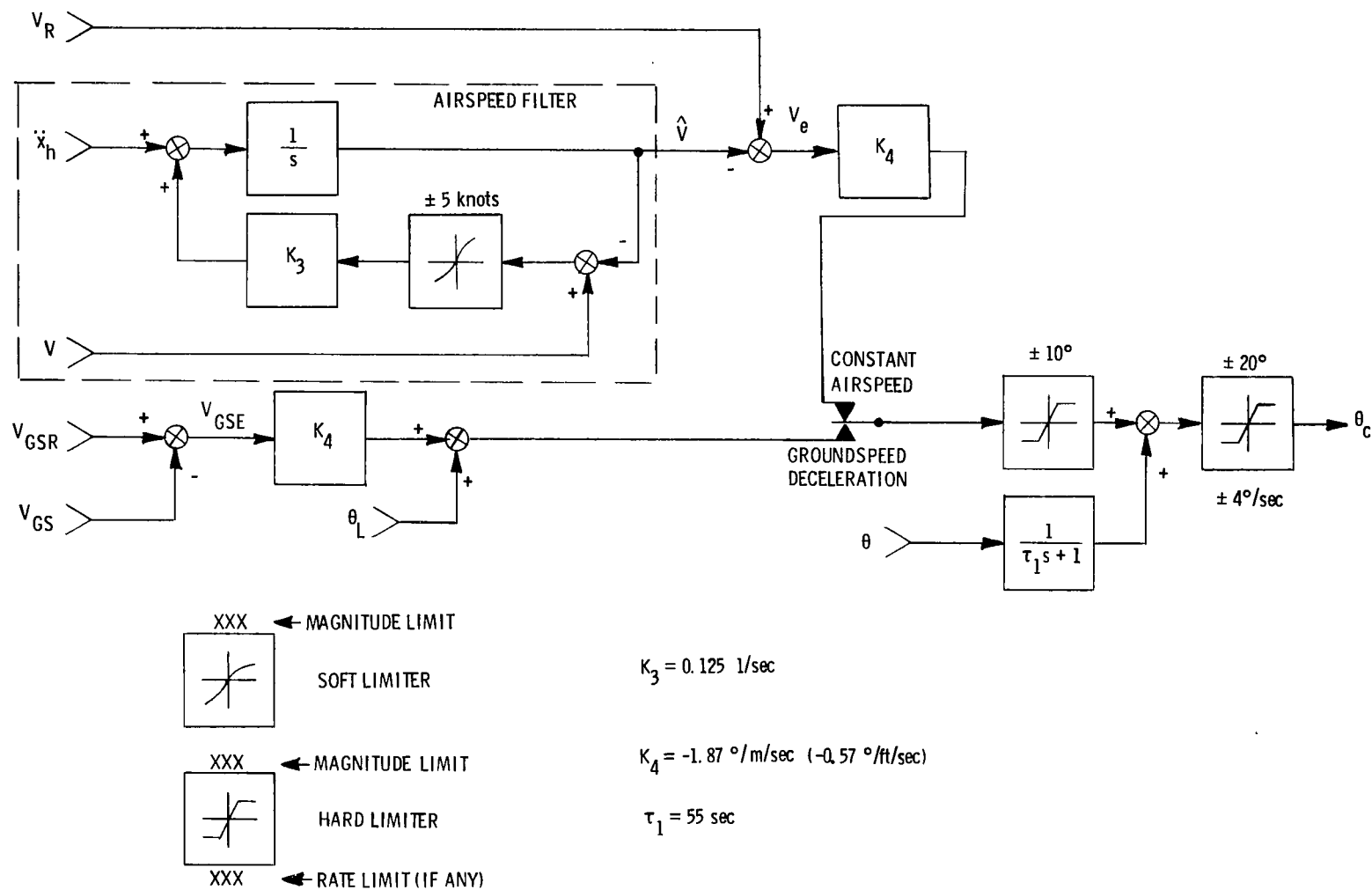
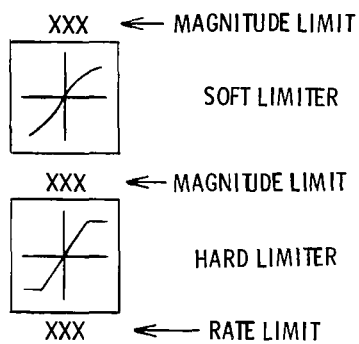
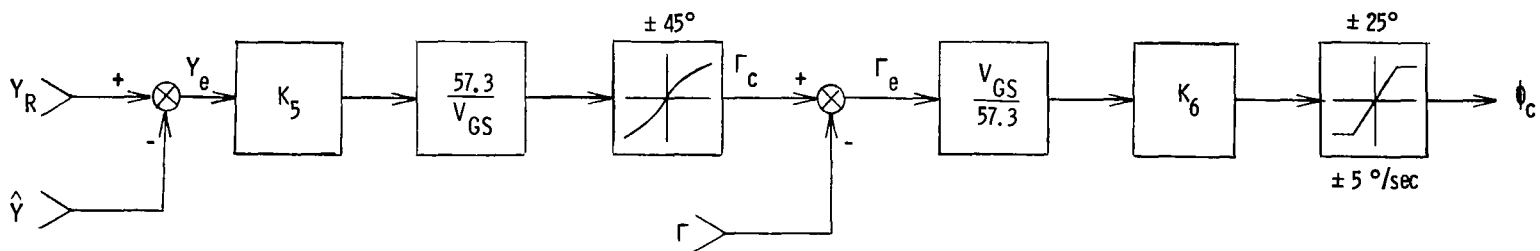


Figure 15.- High-speed pitch command.



$$K_5 = -0.125 \text{ 1/sec}$$

$$K_6 = 1.87 \text{ °/m/sec (0.57 °/ft/sec)}$$

NOTE: CAPTURE LOGIC NOT SHOWN

Figure 16.- High-speed roll command.

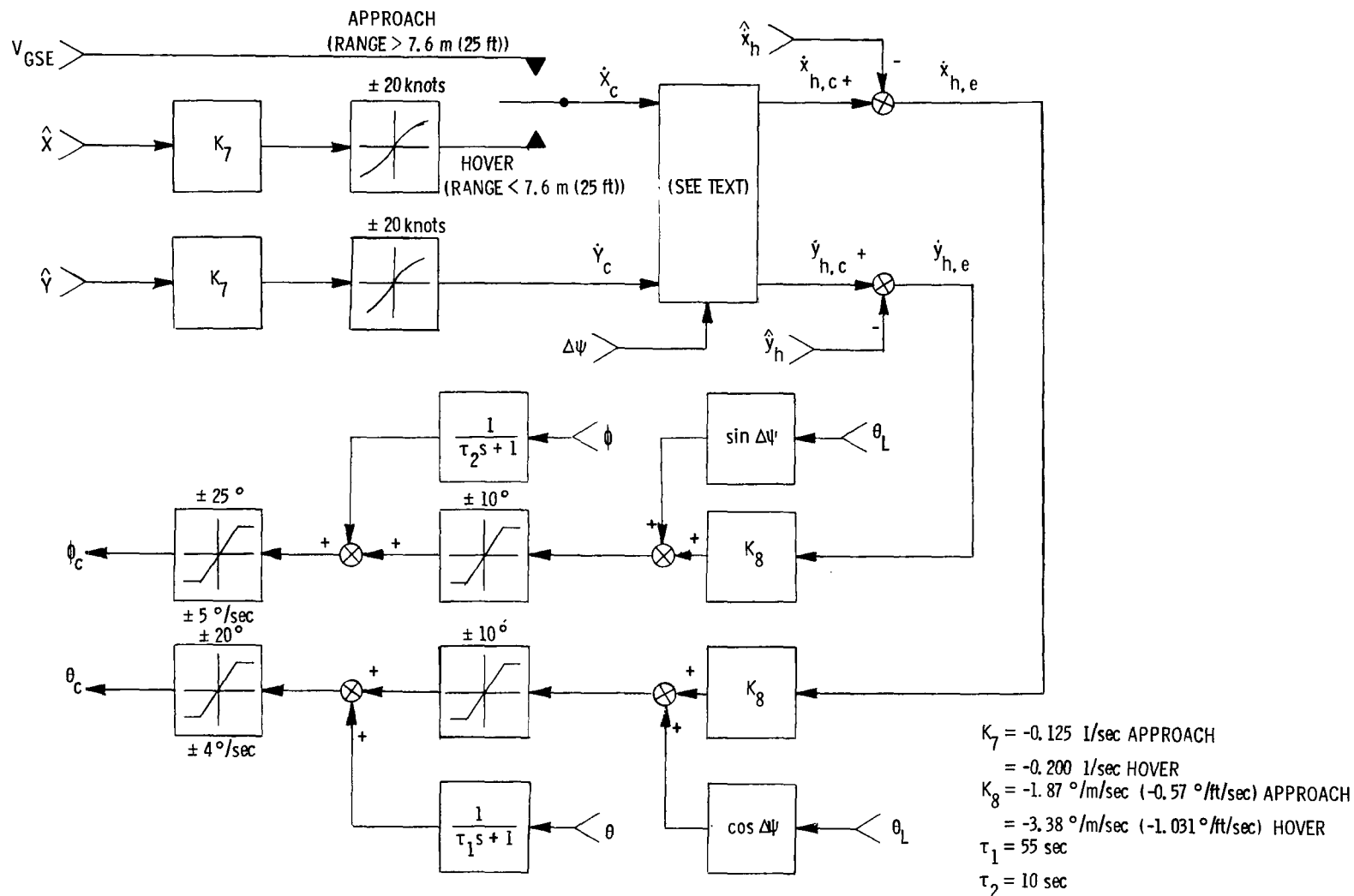
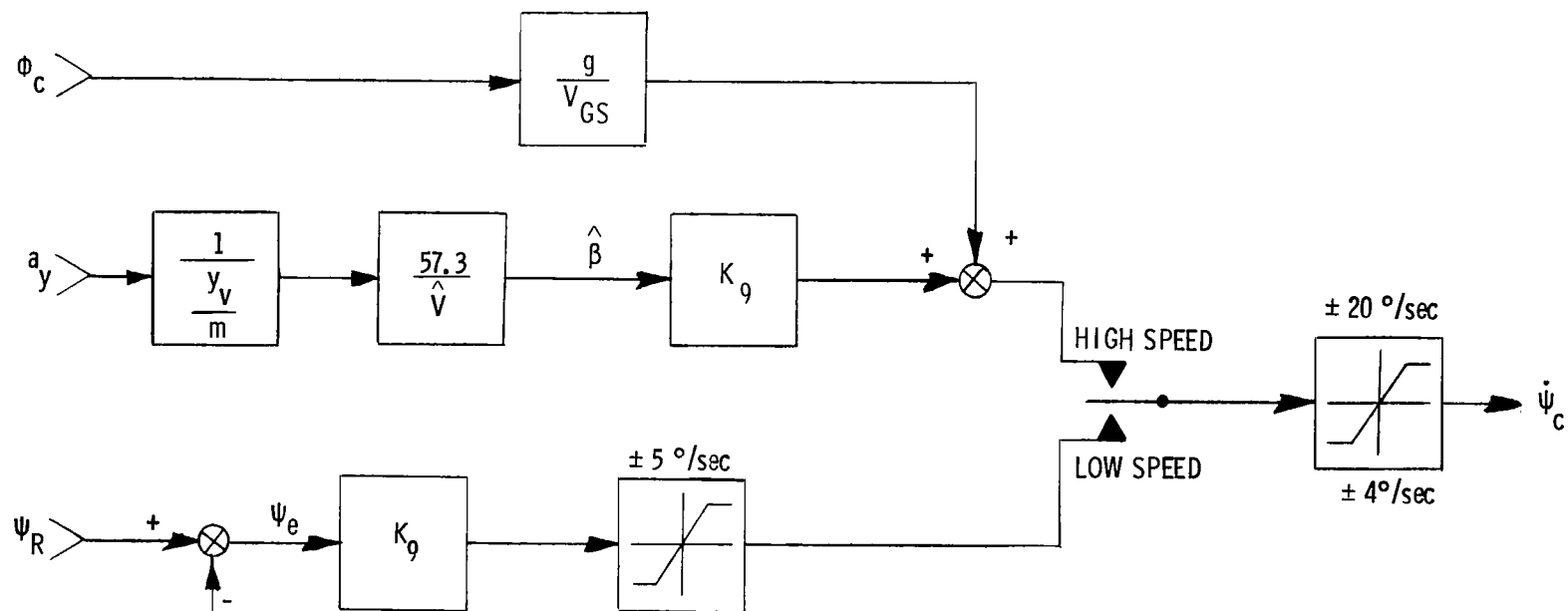


Figure 17.- Low-speed pitch- and roll-command logic.



$$\frac{y_v}{m} = -0.1 \text{ l/sec}$$

$$K_9 = 0.5 \text{ l/sec}$$

Figure 18.- Yaw-command logic.

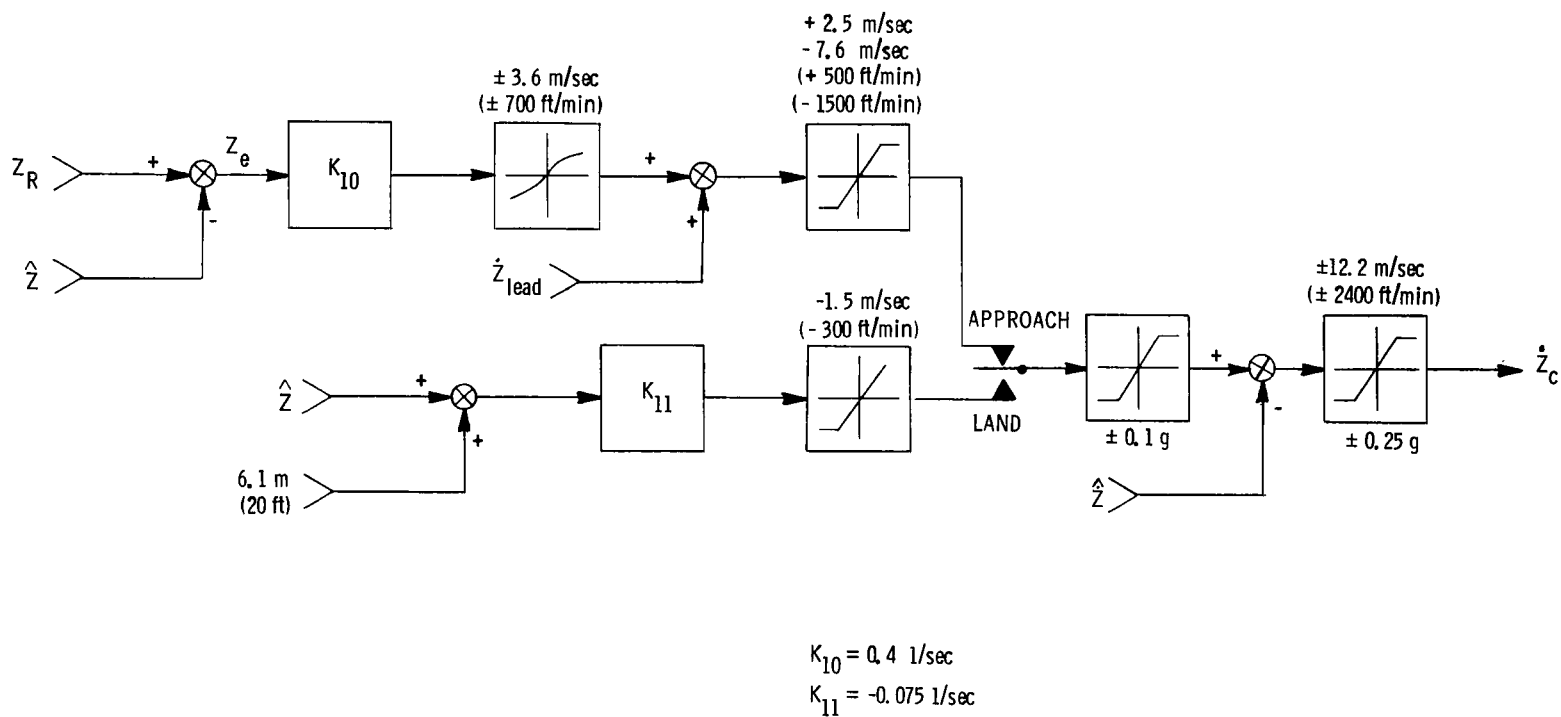


Figure 19.- Power-command logic.

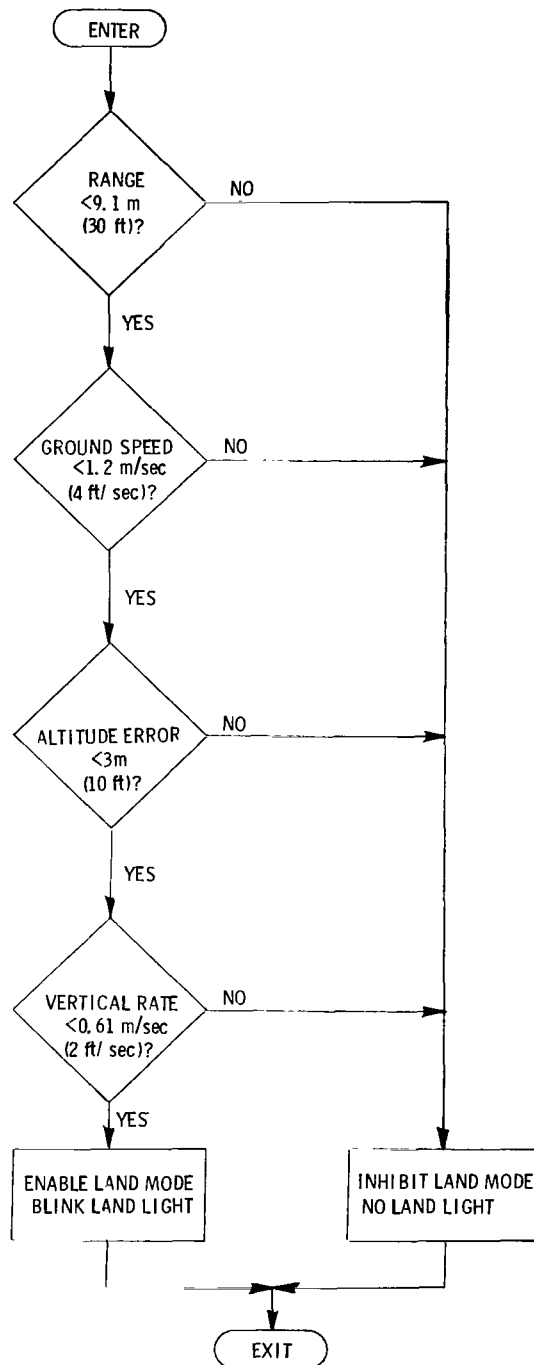


Figure 20.- Landing criteria flow chart.

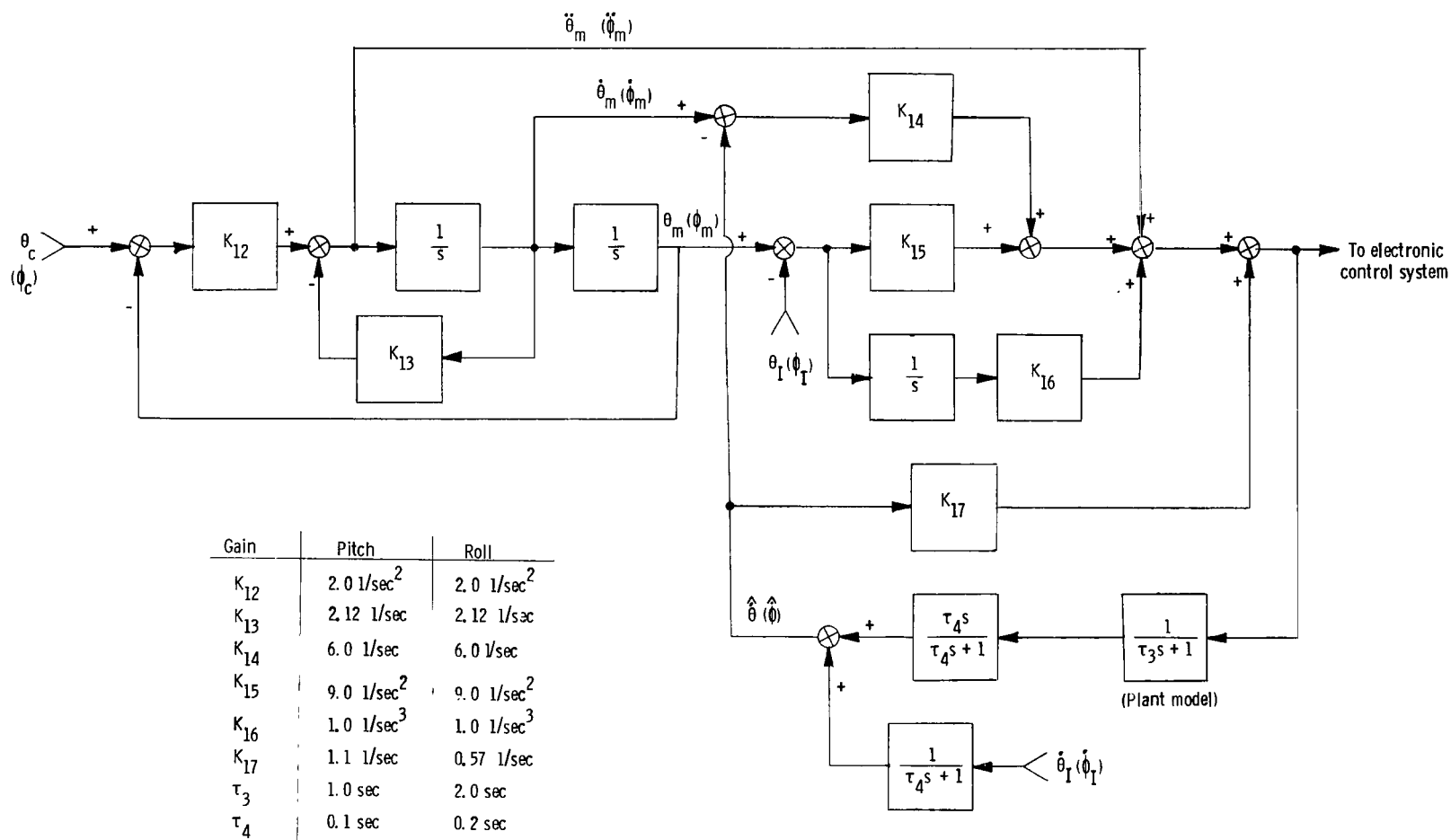


Figure 21.- Pitch and roll inner-loop control.

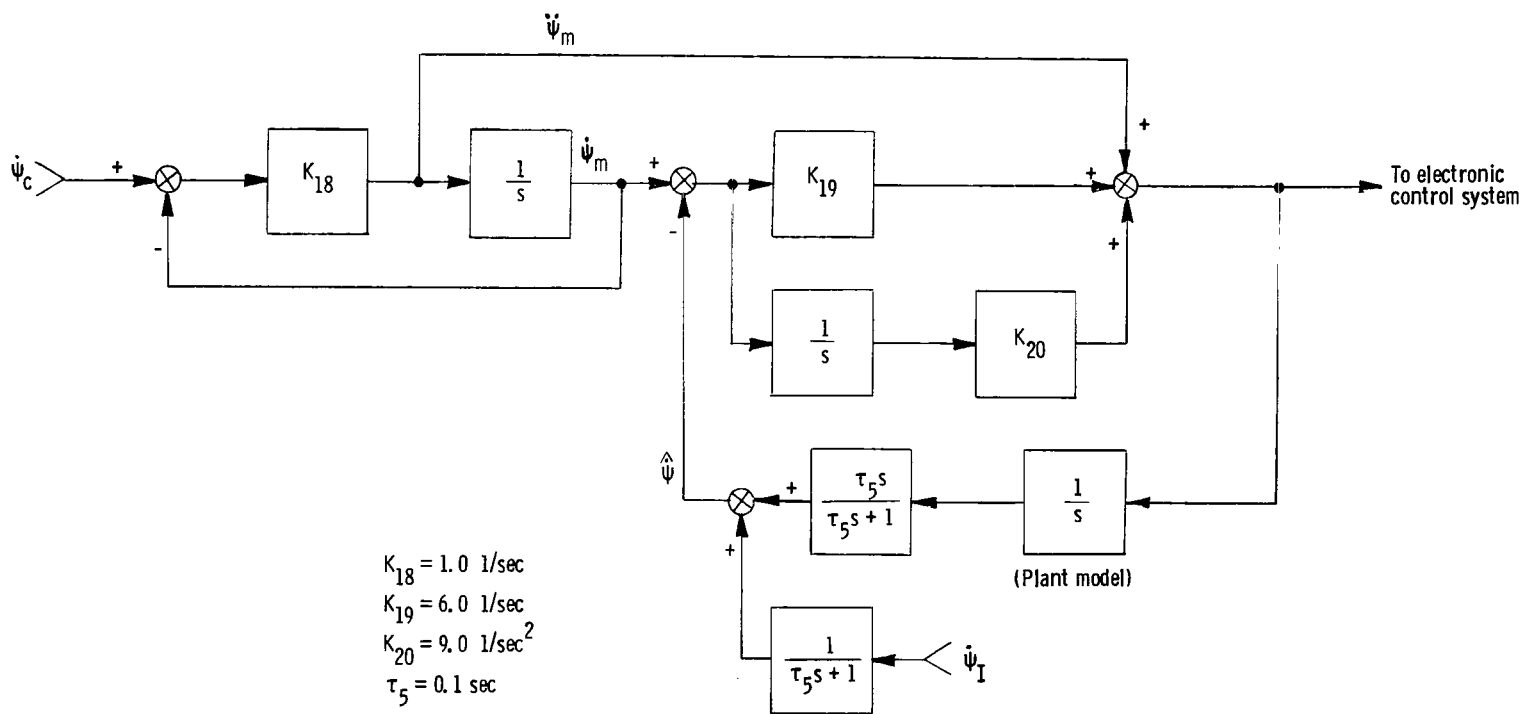
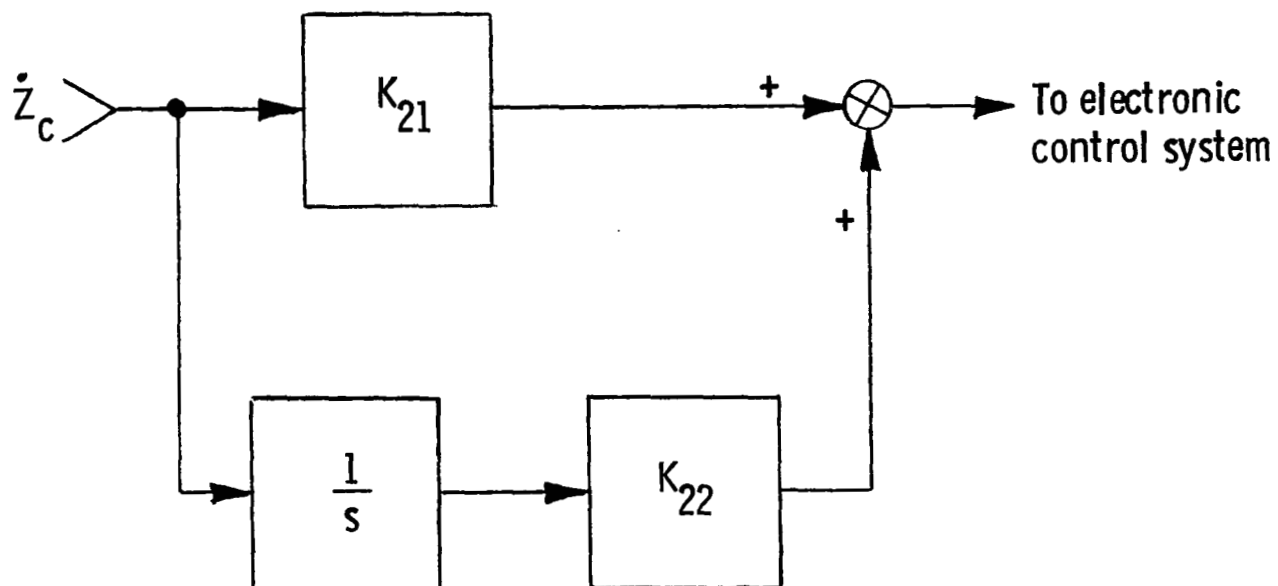


Figure 22.- Yaw inner-loop control.



$$K_{21} = 0.67 \text{ cm/m/sec (0.08 in/ft/sec)}$$

$$K_{22} = 0.133 \text{ cm/m (0.016 in/ft)}$$

Figure 23.- Power inner-loop control.

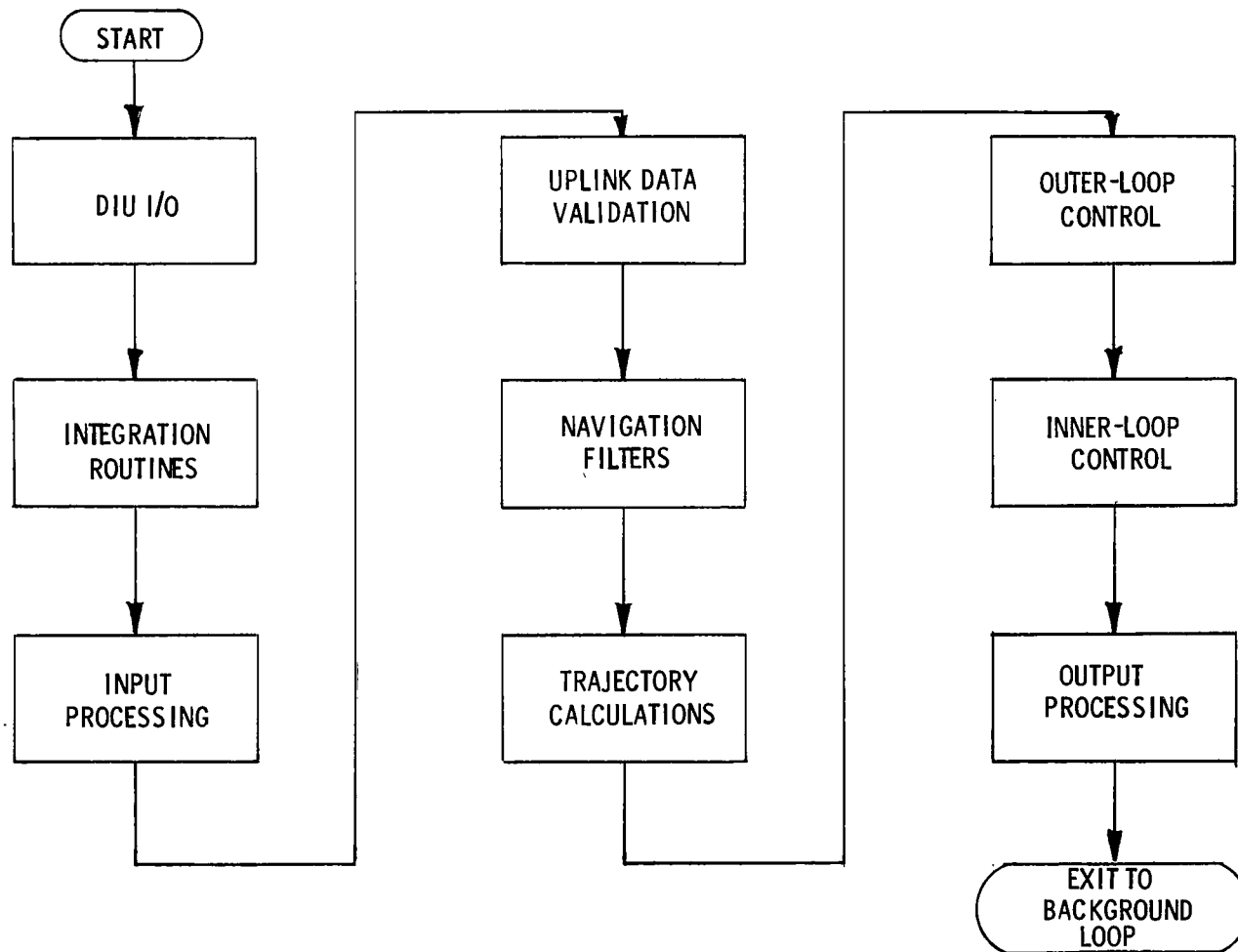


Figure 24.- Sequence of events in real-time loop.

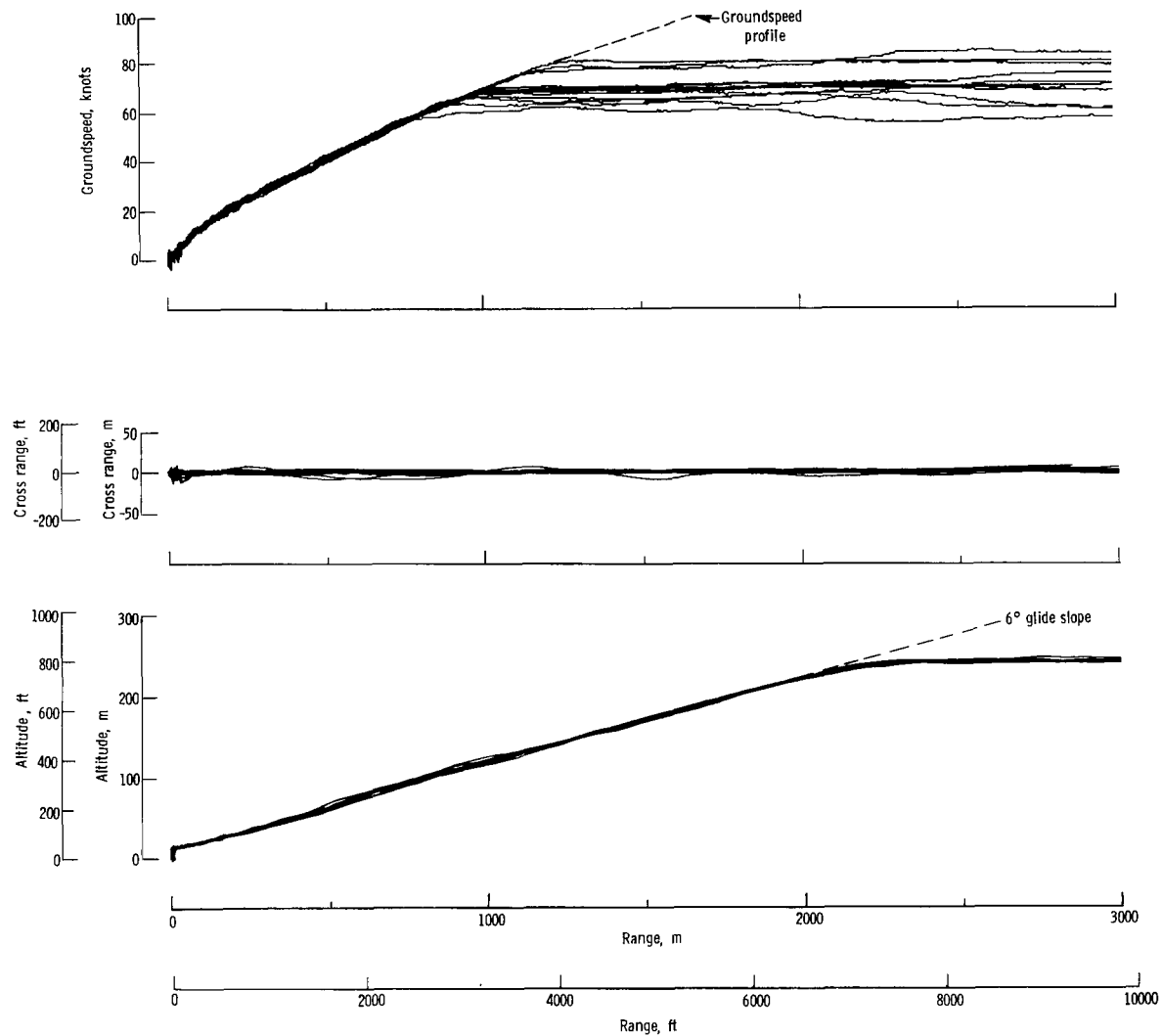


Figure 25.- Automatic landings from first test series.

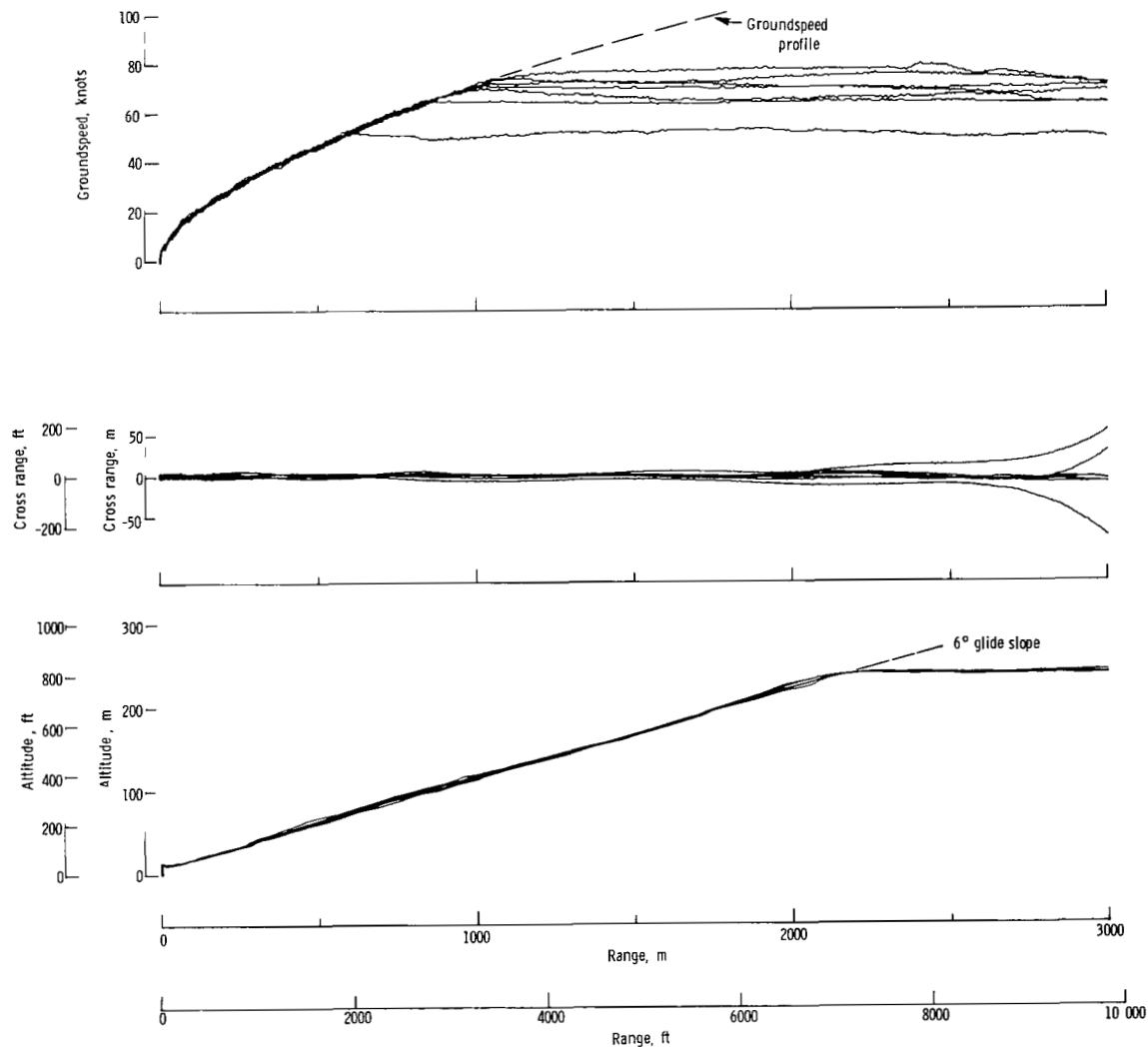


Figure 26.- Automatic landings from second test series.

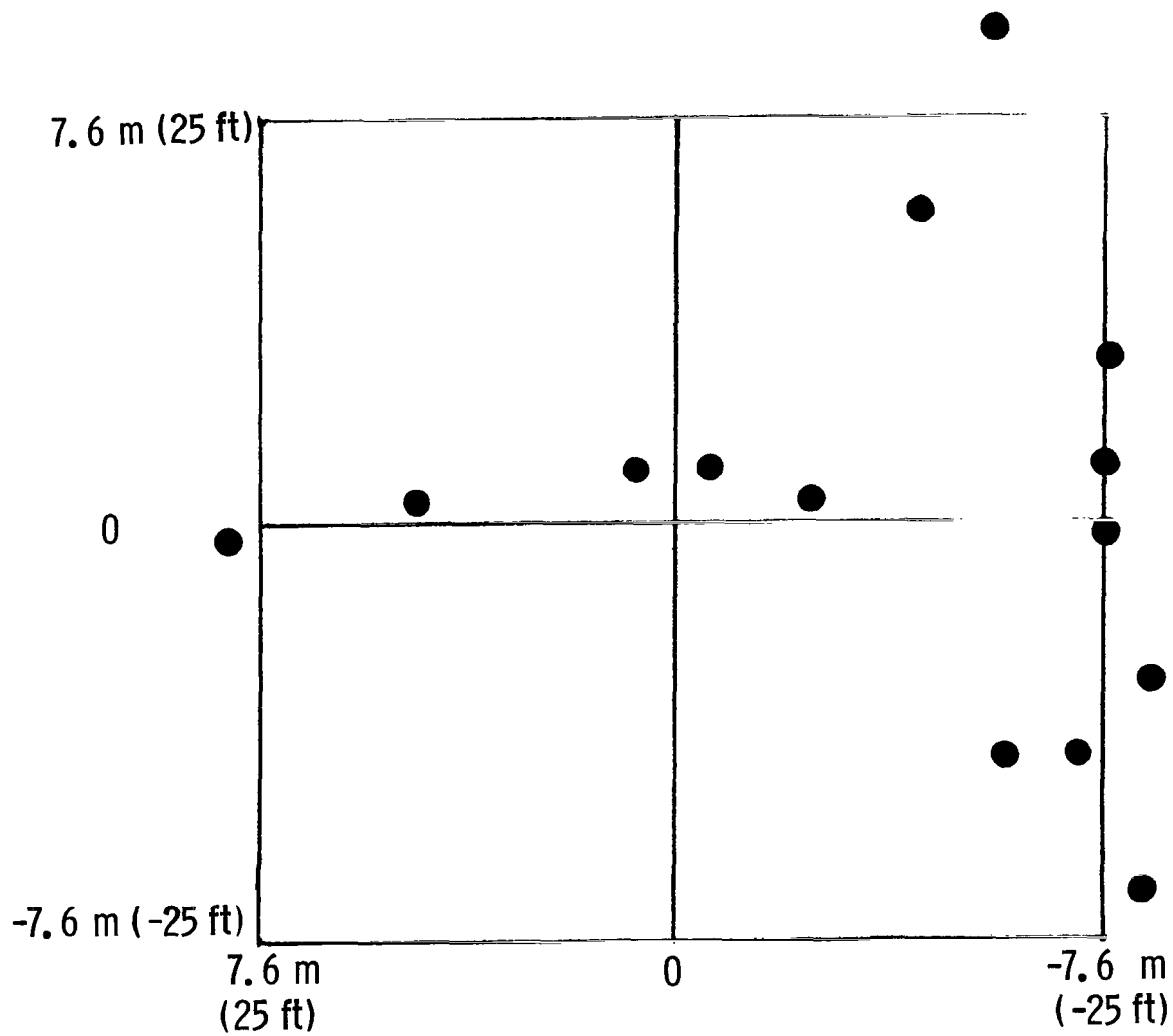


Figure 27.- Touchdown performance in first test series.

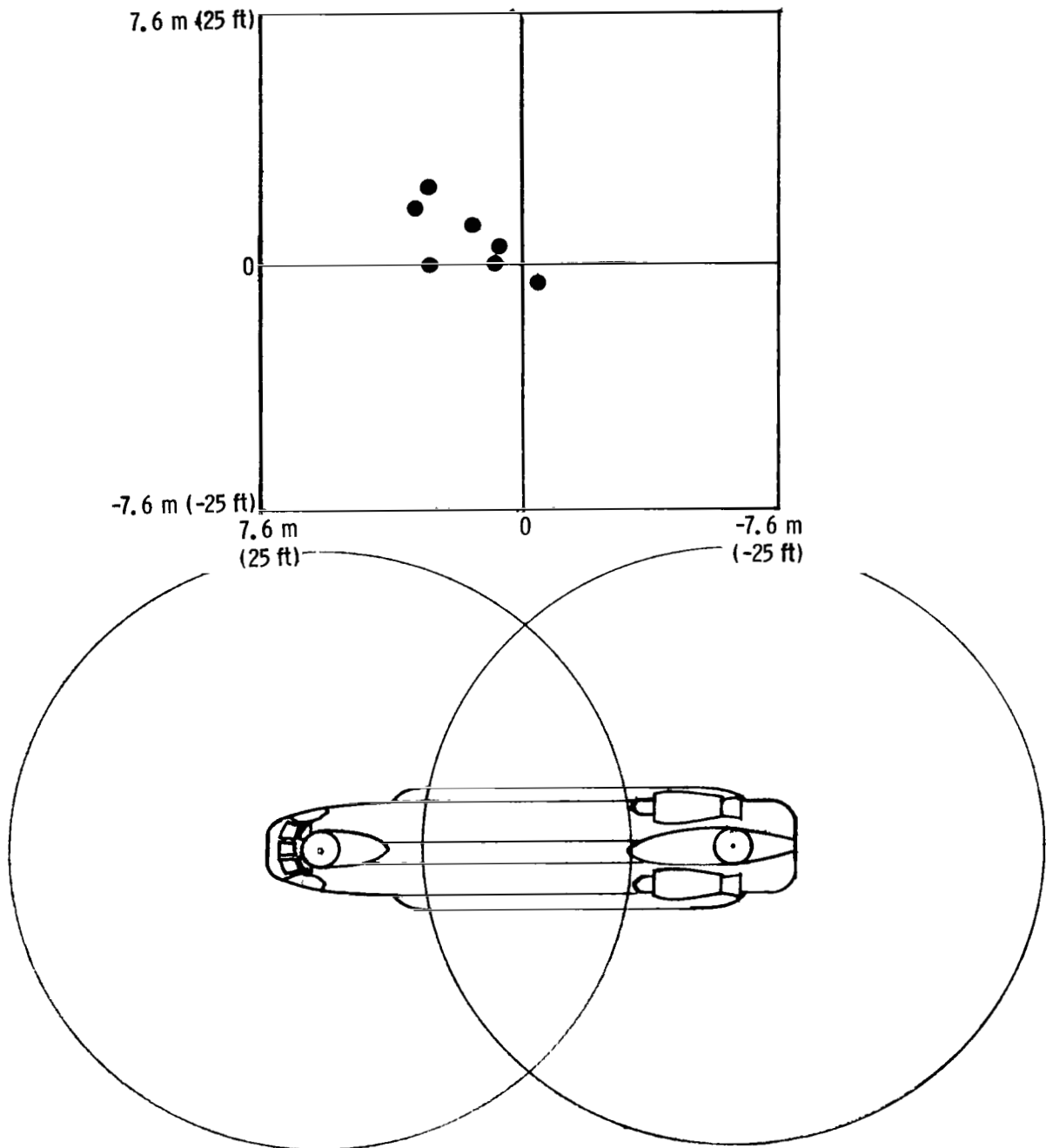


Figure 28.- Touchdown performance in second test series.

1. Report No. NASA TP-1649		2. Government Accession No.		3. Recipient's Catalog No.	
4. Title and Subtitle NAVIGATION, GUIDANCE, AND CONTROL FOR HELICOPTER AUTOMATIC LANDINGS				5. Report Date May 1980	
				6. Performing Organization Code	
7. Author(s) James R. Kelly and Frank R. Niessen				8. Performing Organization Report No. L-13454	
				10. Work Unit No. 534-04-13-57	
9. Performing Organization Name and Address NASA Langley Research Center Hampton, VA 23665				11. Contract or Grant No.	
				13. Type of Report and Period Covered Technical Paper	
12. Sponsoring Agency Name and Address National Aeronautics and Space Administration Washington, DC 20546				14. Sponsoring Agency Code	
15. Supplementary Notes					
16. Abstract A navigation, guidance, and control concept has been developed for helicopter automatic approach and landings. The algorithms employed were implemented in an airborne digital computer installed on a CH-47B research helicopter. Data are shown to illustrate system performance during fully automatic approach and landings in a variety of wind conditions.					
17. Key Words (Suggested by Author(s)) Automatic landings Decelerating approach Helicopter all-weather landings Control algorithms				18. Distribution Statement Unclassified - Unlimited	
				Subject Category 08	
19. Security Classif. (of this report) Unclassified	20. Security Classif. (of this page) Unclassified	21. No. of Pages 55	22. Price* \$5.25		

National Aeronautics and
Space Administration

Washington, D.C.
20546

Official Business

Penalty for Private Use, \$300

THIRD-CLASS BULK RATE

Postage and Fees Paid
National Aeronautics and
Space Administration
NASA-451



6 1 10, A, 042180 S00903DS
DEPT OF THE AIR FORCE
AF WEAPONS LABORATORY
ATTN: TECHNICAL LIBRARY (SUL)
KIRTLAND AFB NM 87117

NASA

POSTMASTER: If Undeliverable (Section 158
Postal Manual) Do Not Return
